

This is the accepted manuscript made available via CHORUS. The article has been published as:

Scaling properties of fractional momentum loss of high- p_{T} hadrons in nucleus-nucleus collisions at $\sqrt{s_{\text{NN}}}$ from 62.4 GeV to 2.76 TeV

A. Adare *et al.* (PHENIX Collaboration)

Phys. Rev. C **93**, 024911 — Published 22 February 2016

DOI: [10.1103/PhysRevC.93.024911](https://doi.org/10.1103/PhysRevC.93.024911)

Scaling properties of fractional momentum loss of high-pT hadrons in nucleus-nucleus collisions at $\sqrt{s_{NN}}$ from 62.4 GeV to 2.76 TeV

- A. Adare,¹³ S. Afanasiev,³² C. Aidala,^{14, 42, 46, 47} N.N. Ajitanand,⁶⁷ Y. Akiba,^{61, 62} R. Akimoto,¹² H. Al-Bataineh,⁵⁵ J. Alexander,⁶⁷ M. Alfred,²⁵ H. Al-Ta'ani,⁵⁵ A. Angerami,¹⁴ K. Aoki,^{35, 38, 61} N. Apadula,^{30, 68} L. Aphecetche,⁶⁹ Y. Aramaki,^{12, 61} R. Armendariz,⁵⁵ S.H. Aronson,⁷ J. Asai,^{61, 62} H. Asano,^{38, 61} E.C. Aschenauer,⁷ E.T. Atomssa,^{39, 68} R. Auerbeck,⁶⁸ T.C. Awes,⁵⁷ B. Azmoun,⁷ V. Babintsev,²⁶ M. Bai,⁶ G. Baksay,²⁰ L. Baksay,²⁰ A. Baldissieri,¹⁶ N.S. Bandara,⁴⁶ B. Bannier,⁶⁸ K.N. Barish,⁸ P.D. Barnes,^{42, *} B. Bassalleck,⁵⁴ A.T. Basye,¹ S. Bathe,^{5, 8, 62} S. Batsouli,⁵⁷ V. Baublis,⁶⁰ C. Baumann,^{7, 48} S. Baumgart,⁶¹ A. Bazilevsky,⁷ M. Beaumier,⁸ S. Beckman,¹³ S. Belikov,^{7, *} R. Belmont,^{13, 47, 73} R. Bennett,⁶⁸ A. Berdnikov,⁶⁴ Y. Berdnikov,⁶⁴ A.A. Bickley,¹³ D.S. Blau,³⁷ J.G. Boissevain,⁴² J.S. Bok,^{54, 55, 77} H. Borel,¹⁶ K. Boyle,^{62, 68} M.L. Brooks,⁴² J. Bryslawskyj,⁵ H. Buesching,⁷ V. Bumazhnov,²⁶ G. Bunce,^{7, 62} S. Butsyk,^{42, 54, 68} C.M. Camacho,⁴² S. Campbell,^{14, 30, 68} P. Castera,⁶⁸ B.S. Chang,⁷⁷ J.-L. Charvet,¹⁶ C.-H. Chen,^{62, 68} S. Chernichenko,²⁶ C.Y. Chi,¹⁴ J. Chiba,³⁵ M. Chiu,^{7, 27} I.J. Choi,^{27, 77} J.B. Choi,¹⁰ S. Choi,⁶⁶ R.K. Choudhury,⁴ P. Christiansen,⁴⁴ T. Chujo,^{72, 73} P. Chung,⁶⁷ A. Churny,²⁶ O. Chvala,⁸ V. Cianciolo,⁵⁷ Z. Citron,^{68, 75} C.R. Cleven,²² B.A. Cole,¹⁴ M.P. Comets,⁵⁸ M. Connors,⁶⁸ P. Constantin,⁴² M. Csanád,¹⁸ T. Csörgő,⁷⁶ T. Dahms,⁶⁸ S. Dairaku,^{38, 61} I. Danchev,⁷³ D. Danley,⁵⁶ K. Das,²¹ A. Datta,^{46, 54} M.S. Daugherty,¹ G. David,⁷ M.B. Deaton,¹ K. DeBlasio,⁵⁴ K. Dehmelt,^{20, 68} H. Delagrange,^{69, *} A. Denisov,²⁶ D. d'Enterria,¹⁴ A. Deshpande,^{62, 68} E.J. Desmond,⁷ K.V. Dharmawardane,⁵⁵ O. Dietzsch,⁶⁵ L. Ding,³⁰ A. Dion,^{30, 68} P.B. Diss,⁴⁵ J.H. Do,⁷⁷ M. Donadelli,⁶⁵ L. D'Orazio,⁴⁵ O. Drapier,³⁹ A. Drees,⁶⁸ K.A. Drees,⁶ A.K. Dubey,⁷⁵ J.M. Durham,^{42, 68} A. Durum,²⁶ D. Dutta,⁴ V. Dzhordzhadze,⁸ S. Edwards,^{6, 21} Y.V. Efremenko,⁵⁷ J. Egdemir,⁶⁸ F. Ellinghaus,¹³ W.S. Emam,⁸ T. Engelmire,¹⁴ A. Enokizono,^{41, 57, 61, 63} H. En'yo,^{61, 62} S. Esumi,⁷² K.O. Eyser,^{7, 8} B. Fadern,⁴⁹ N. Feege,⁶⁸ D.E. Fields,^{54, 62} M. Finger,^{9, 32} M. Finger, Jr.,^{9, 32} F. Fleuret,³⁹ S.L. Fokin,³⁷ Z. Fraenkel,^{75, *} J.E. Frantz,^{56, 68} A. Franz,⁷ A.D. Frawley,²¹ K. Fujiwara,⁶¹ Y. Fukao,^{38, 61} T. Fusayasu,⁵¹ S. Gadrat,⁴³ K. Ganev,¹ C. Gal,⁶⁸ P. Gallus,¹⁵ P. Garg,³ A. Garishvili,⁷⁰ I. Garishvili,^{41, 70} H. Ge,⁶⁸ F. Giordano,²⁷ A. Glenn,^{13, 41} H. Gong,⁶⁸ X. Gong,⁶⁷ M. Gonin,³⁹ J. Gosset,¹⁶ Y. Goto,^{61, 62} R. Granier de Cassagnac,³⁹ N. Grau,^{2, 14, 30} S.V. Greene,⁷³ M. Grosse Perdekamp,^{27, 62} T. Gunji,¹² L. Guo,⁴² H.-A. Gustafsson,^{44, *} T. Hachiya,^{24, 61} A. Hadj Henni,⁶⁹ C. Haegemann,⁵⁴ J.S. Haggerty,⁷ K.I. Hahn,¹⁹ H. Hamagaki,¹² J. Hamblen,⁷⁰ H.F. Hamilton,¹ R. Han,⁵⁹ S.Y. Han,¹⁹ J. Hanks,^{14, 68} H. Harada,²⁴ E.P. Hartouni,⁴¹ K. Haruna,²⁴ S. Hasegawa,³¹ T.O.S. Haseler,²² K. Hashimoto,^{61, 63} E. Haslum,⁴⁴ R. Hayano,¹² X. He,²² M. Heffner,⁴¹ T.K. Hemmick,⁶⁸ T. Hester,⁸ H. Hiejima,²⁷ J.C. Hill,³⁰ R. Hobbs,⁵⁴ M. Hohlmann,²⁰ R.S. Hollis,⁸ W. Holzmann,^{14, 67} K. Homma,²⁴ B. Hong,³⁶ T. Horaguchi,^{24, 61, 71, 72} Y. Hori,¹² D. Hornback,⁷⁰ T. Hoshino,²⁴ N. Hotvedt,³⁰ J. Huang,⁷ S. Huang,⁷³ T. Ichihara,^{61, 62} R. Ichimiya,⁶¹ J. Ide,⁴⁹ H. Iinuma,^{35, 38, 61} Y. Ikeda,^{61, 72} K. Imai,^{31, 38, 61} J. Imrek,¹⁷ M. Inaba,⁷² Y. Inoue,^{61, 63} A. Iordanova,⁸ D. Isenhowe,¹ L. Isenhowe,¹ M. Ishihara,⁶¹ T. Isobe,^{12, 61} M. Issah,^{67, 73} A. Isupov,³² D. Ivanishchev,⁶⁰ B.V. Jacak,⁶⁸ M. Javani,²² M. Jezghani,²² J. Jia,^{7, 14, 67} X. Jiang,⁴² J. Jin,¹⁴ O. Jinnouchi,⁶² B.M. Johnson,⁷ K.S. Joo,⁵⁰ D. Jouan,⁵⁸ D.S. Jumper,^{1, 27} F. Kajihara,¹² S. Kametani,^{12, 61, 74} N. Kamihara,^{61, 62} J. Kamin,⁶⁸ S. Kanda,¹² M. Kaneta,⁶² S. Kaneti,⁶⁸ B.H. Kang,²³ J.H. Kang,⁷⁷ J.S. Kang,²³ H. Kanou,^{61, 71} J. Kapustinsky,⁴² K. Karatsu,^{38, 61} M. Kasai,^{61, 63} D. Kawall,^{46, 62} M. Kawashima,^{61, 63} A.V. Kazantsev,³⁷ T. Kempel,³⁰ J.A. Key,⁵⁴ V. Khachatryan,⁶⁸ A. Khanzadeev,⁶⁰ K.M. Kijima,²⁴ J. Kikuchi,⁷⁴ B.I. Kim,³⁶ C. Kim,³⁶ D.H. Kim,⁵⁰ D.J. Kim,^{33, 77} E. Kim,⁶⁶ E.-J. Kim,¹⁰ G.W. Kim,¹⁹ H.J. Kim,⁷⁷ K.-B. Kim,¹⁰ M. Kim,⁶⁶ S.H. Kim,⁷⁷ Y.-J. Kim,²⁷ Y.K. Kim,²³ B. Kimelman,⁴⁹ E. Kinney,¹³ K. Kiriluk,¹³ Á. Kiss,¹⁸ E. Kistenev,⁷ R. Kitamura,¹² A. Kiyomichi,⁶¹ J. Klatsky,²¹ J. Klay,⁴¹ C. Klein-Boesing,⁴⁸ D. Kleinjan,⁸ P. Kline,⁶⁸ T. Koblesky,¹³ L. Kochenda,⁶⁰ V. Kochetkov,²⁶ Y. Komatsu,^{12, 35} B. Komkov,⁶⁰ M. Konno,⁷² J. Koster,²⁷ D. Kotchetkov,^{8, 54, 56} D. Kotov,^{60, 64} A. Kozlov,⁷⁵ A. Král,¹⁵ A. Kravitz,¹⁴ F. Krizek,³³ J. Kubart,^{9, 29} G.J. Kunde,⁴² N. Kurihara,¹² K. Kurita,^{61, 63} M. Kurosawa,^{61, 62} M.J. Kwon,³⁶ Y. Kwon,^{70, 77} G.S. Kyle,⁵⁵ R. Lacey,⁶⁷ Y.S. Lai,¹⁴ J.G. Lajoie,³⁰ A. Lebedev,³⁰ B. Lee,²³ D.M. Lee,⁴² J. Lee,¹⁹ K. Lee,⁶⁶ K.B. Lee,³⁶ K.S. Lee,³⁶ M.K. Lee,⁷⁷ S. Lee,⁷⁷ S.H. Lee,⁶⁸ S.R. Lee,¹⁰ T. Lee,⁶⁶ M.J. Leitch,⁴² M.A.L. Leite,⁶⁵ M. Leitgab,²⁷ E. Leitner,⁷³ B. Lenzi,⁶⁵ B. Lewis,⁶⁸ X. Li,¹¹ P. Liebing,⁶² S.H. Lim,⁷⁷ L.A. Linden Levy,¹³ T. Liška,¹⁵ A. Litvinenko,³² H. Liu,^{42, 55} M.X. Liu,⁴² B. Love,⁷³ R. Luechtenborg,⁴⁸ D. Lynch,⁷ C.F. Maguire,⁷³ Y.I. Makdisi,⁶ M. Makey,^{75, 78} A. Malakhov,³² M.D. Malik,⁵⁴ A. Manion,⁶⁸ V.I. Manko,³⁷ E. Mannel,^{7, 14} Y. Mao,^{59, 61} L. Mašek,^{9, 29} H. Masui,⁷² S. Masumoto,^{12, 35} F. Matathias,¹⁴ M. McCumber,^{13, 42, 68} P.L. McGaughey,⁴² D. McGlinchey,^{13, 21} C. McKinney,²⁷ N. Means,⁶⁸ A. Meles,⁵⁵ M. Mendoza,⁸ B. Meredith,²⁷ Y. Miake,⁷² T. Mibe,³⁵ A.C. Mignerey,⁴⁵ P. Mikeš,^{9, 29} K. Miki,^{61, 72} T.E. Miller,⁷³ A. Milov,^{7, 68, 75} S. Mioduszewski,⁷ D.K. Mishra,⁴ M. Mishra,³ J.T. Mitchell,⁷ M. Mitrovski,⁶⁷ Y. Miyachi,^{61, 71} S. Miyasaka,^{61, 71}

S. Mizuno,^{61,72} A.K. Mohanty,⁴ S. Mohapatra,⁶⁷ P. Montuenga,²⁷ H.J. Moon,⁵⁰ T. Moon,⁷⁷ Y. Morino,¹²
A. Morreale,⁸ D.P. Morrison,^{7,†} S. Motschwiller,⁴⁹ T.V. Moukhanova,³⁷ D. Mukhopadhyay,⁷³ T. Murakami,^{38,61}
J. Murata,^{61,63} A. Mwai,⁶⁷ T. Nagae,³⁸ S. Nagamiya,^{35,61} K. Nagashima,²⁴ Y. Nagata,⁷² J.L. Nagle,^{13,‡}
M. Naglis,⁷⁵ M.I. Nagy,^{18,76} I. Nakagawa,^{61,62} H. Nakagomi,^{61,72} Y. Nakamiya,²⁴ K.R. Nakamura,^{38,61}
T. Nakamura,^{24,35,61} K. Nakano,^{61,71} C. Nattrass,⁷⁰ A. Nederlof,⁴⁹ P.K. Netrakanti,⁴ J. Newby,⁴¹ M. Nguyen,⁶⁸
M. Nihashi,^{24,61} T. Niida,⁷² S. Nishimura,¹² B.E. Norman,⁴² R. Nouicer,^{7,62} T. Novak,^{34,76} N. Novitzky,^{33,68}
A.S. Nyanin,³⁷ E. O'Brien,⁷ S.X. Oda,¹² C.A. Ogilvie,³⁰ H. Ohnishi,⁶¹ M. Oka,⁷² K. Okada,⁶² O.O. Omiwade,¹
Y. Onuki,⁶¹ J.D. Orjuela Koop,¹³ J.D. Osborn,⁴⁷ A. Oskarsson,⁴⁴ M. Ouchida,^{24,61} K. Ozawa,^{12,35} R. Pak,⁷
D. Pal,⁷³ A.P.T. Palounek,⁴² V. Pantuev,^{28,68} V. Papavassiliou,⁵⁵ B.H. Park,²³ I.H. Park,¹⁹ J. Park,⁶⁶ J.S. Park,⁶⁶
S. Park,⁶⁶ S.K. Park,³⁶ W.J. Park,³⁶ S.F. Pate,⁵⁵ L. Patel,²² M. Patel,³⁰ H. Pei,³⁰ J.-C. Peng,²⁷ H. Pereira,¹⁶
D.V. Perepelitsa,^{7,14} G.D.N. Perera,⁵⁵ V. Peresedov,³² D.Yu. Peressounko,³⁷ J. Perry,³⁰ R. Petti,^{7,68}
C. Pinkenburg,⁷ R. Pinson,¹ R.P. Pisani,⁷ M. Proissl,⁶⁸ M.L. Purschke,⁷ A.K. Purwar,⁴² H. Qu,^{1,22} J. Rak,^{33,54}
A. Rakotozafindrabe,³⁹ B.J. Ramson,⁴⁷ I. Ravinovich,⁷⁵ K.F. Read,^{57,70} S. Rembeczki,²⁰ M. Reuter,⁶⁸ K. Reygers,⁴⁸
D. Reynolds,⁶⁷ V. Riabov,^{53,60} Y. Riabov,^{60,64} E. Richardson,⁴⁵ T. Rinn,³⁰ D. Roach,⁷³ G. Roche,^{43,*}
S.D. Rolnick,⁸ A. Romana,^{39,*} M. Rosati,³⁰ C.A. Rosen,¹³ S.S.E. Rosendahl,⁴⁴ P. Rosnet,⁴³ Z. Rowan,⁵
J.G. Rubin,⁴⁷ P. Rukoyatkin,³² P. Ružička,²⁹ V.L. Rykov,⁶¹ B. Sahlmueller,^{48,68} N. Saito,^{35,38,61,62} T. Sakaguchi,⁷
S. Sakai,⁷² K. Sakashita,^{61,71} H. Sakata,²⁴ H. Sako,³¹ V. Samsonov,^{53,60} M. Sano,⁷² S. Sano,^{12,74} M. Sarsour,²²
S. Sato,^{31,35} T. Sato,⁷² S. Sawada,³⁵ B. Schaefer,⁷³ B.K. Schmoll,⁷⁰ K. Sedgwick,⁸ J. Seele,¹³ R. Seidl,^{27,61,62}
A.Yu. Semenov,³⁰ V. Semenov,²⁶ A. Sen,^{22,70} R. Seto,⁸ P. Sett,⁴ A. Sexton,⁴⁵ D. Sharma,^{68,75} I. Shein,²⁶
A. Shevel,^{60,67} T.-A. Shibata,^{61,71} K. Shigaki,²⁴ M. Shimomura,^{30,52,72} K. Shoji,^{38,61} P. Shukla,⁴ A. Sickles,^{7,27,68}
C.L. Silva,^{30,42,65} D. Silvermyr,^{44,57} C. Silvestre,¹⁶ K.S. Sim,³⁶ B.K. Singh,³ C.P. Singh,³ V. Singh,³ S. Skutnik,³⁰
M. Slunečka,^{9,32} M. Snowball,⁴² A. Soldatov,²⁶ R.A. Soltz,⁴¹ W.E. Sondheim,⁴² S.P. Sorensen,⁷⁰ I.V. Sourikova,⁷
N.A. Sparks,¹ F. Staley,¹⁶ P.W. Stankus,⁵⁷ E. Stenlund,⁴⁴ M. Stepanov,^{46,55,*} A. Ster,⁷⁶ S.P. Stoll,⁷ T. Sugitate,²⁴
C. Suire,⁵⁸ A. Sukhanov,⁷ T. Sumita,⁶¹ J. Sun,⁶⁸ J. Sziklai,⁷⁶ T. Tabaru,⁶² S. Takagi,⁷² E.M. Takagui,⁶⁵
A. Takahara,¹² A. Taketani,^{61,62} R. Tanabe,⁷² Y. Tanaka,⁵¹ S. Taneja,⁶⁸ K. Tanida,^{38,61,62,66} M.J. Tannenbaum,⁷
S. Tarafdar,^{3,75} A. Taranenko,^{53,67} P. Tarján,¹⁷ E. Tennant,⁵⁵ H. Themann,⁶⁸ T.L. Thomas,⁵⁴ R. Tieulent,²²
A. Timilsina,³⁰ T. Todoroki,^{61,72} M. Togawa,^{38,61} A. Toia,⁶⁸ J. Tojo,⁶¹ L. Tomášek,²⁹ M. Tomášek,^{15,29}
H. Torii,^{24,61} C.L. Towell,¹ R. Towell,¹ R.S. Towell,¹ V.-N. Tram,³⁹ I. Tserruya,⁷⁵ Y. Tsuchimoto,^{12,24}
T. Tsuji,¹² C. Vale,^{7,30} H. Valle,⁷³ H.W. van Hecke,⁴² M. Vargyas,¹⁸ E. Vazquez-Zambrano,¹⁴ A. Veicht,^{14,27}
J. Velkovska,⁷³ R. Vértesi,^{17,76} A.A. Vinogradov,³⁷ M. Virius,¹⁵ A. Vossen,²⁷ V. Vrba,^{15,29} E. Vznuzdaev,⁶⁰
M. Wagner,^{38,61} D. Walker,⁶⁸ X.R. Wang,^{55,62} D. Watanabe,²⁴ K. Watanabe,⁷² Y. Watanabe,^{61,62}
Y.S. Watanabe,^{12,35} F. Wei,^{30,55} R. Wei,⁶⁷ J. Wessels,⁴⁸ A.S. White,⁴⁷ S.N. White,⁷ D. Winter,¹⁴
S. Wolin,²⁷ J.P. Wood,¹ C.L. Woody,⁷ R.M. Wright,¹ M. Wysocki,^{13,57} B. Xia,⁵⁶ W. Xie,⁶² L. Xue,²²
S. Yalcin,⁶⁸ Y.L. Yamaguchi,^{12,61,68,74} K. Yamaura,²⁴ R. Yang,²⁷ A. Yanovich,²⁶ Z. Yasin,⁸ J. Ying,²²
S. Yokkaichi,^{61,62} J.H. Yoo,³⁶ I. Yoon,⁶⁶ Z. You,^{42,59} G.R. Young,⁵⁷ I. Younus,^{40,54} H. Yu,⁵⁹ I.E. Yushmanov,³⁷
W.A. Zajc,¹⁴ O. Zaudtke,⁴⁸ A. Zelenski,⁶ C. Zhang,⁵⁷ S. Zhou,¹¹ J. Zimanyi,^{76,*} L. Zolin,³² and L. Zou⁸

(PHENIX Collaboration)

¹Abilene Christian University, Abilene, Texas 79699, USA

²Department of Physics, Augustana University, Sioux Falls, South Dakota 57197, USA

³Department of Physics, Banaras Hindu University, Varanasi 221005, India

⁴Bhabha Atomic Research Centre, Bombay 400 085, India

⁵Baruch College, City University of New York, New York, New York, 10010 USA

⁶Collider-Accelerator Department, Brookhaven National Laboratory, Upton, New York 11973-5000, USA

⁷Physics Department, Brookhaven National Laboratory, Upton, New York 11973-5000, USA

⁸University of California-Riverside, Riverside, California 92521, USA

⁹Charles University, Ovocný trh 5, Praha 1, 116 36, Prague, Czech Republic

¹⁰Chonbuk National University, Jeonju, 561-756, Korea

¹¹Science and Technology on Nuclear Data Laboratory, China Institute of Atomic Energy, Beijing 102413, P. R. China

¹²Center for Nuclear Study, Graduate School of Science, University of Tokyo, 7-3-1 Hongo, Bunkyo, Tokyo 113-0033, Japan

¹³University of Colorado, Boulder, Colorado 80309, USA

¹⁴Columbia University, New York, New York 10027 and Nevis Laboratories, Irvington, New York 10533, USA

¹⁵Czech Technical University, Zikova 4, 166 36 Prague 6, Czech Republic

¹⁶Dapnia, CEA Saclay, F-91191, Gif-sur-Yvette, France

¹⁷Debrecen University, H-4010 Debrecen, Egyetem tér 1, Hungary

¹⁸ELTE, Eötvös Loránd University, H-1117 Budapest, Pázmány P. s. 1/A, Hungary

¹⁹Ewha Womans University, Seoul 120-750, Korea

- ²⁰Florida Institute of Technology, Melbourne, Florida 32901, USA
²¹Florida State University, Tallahassee, Florida 32306, USA
²²Georgia State University, Atlanta, Georgia 30303, USA
²³Hanyang University, Seoul 133-792, Korea
²⁴Hiroshima University, Kagamiyama, Higashi-Hiroshima 739-8526, Japan
²⁵Department of Physics and Astronomy, Howard University, Washington, DC 20059, USA
²⁶IHEP Protvino, State Research Center of Russian Federation, Institute for High Energy Physics, Protvino, 142281, Russia
²⁷University of Illinois at Urbana-Champaign, Urbana, Illinois 61801, USA
²⁸Institute for Nuclear Research of the Russian Academy of Sciences, prospekt 60-letiya Oktyabrya 7a, Moscow 117312, Russia
²⁹Institute of Physics, Academy of Sciences of the Czech Republic, Na Slovance 2, 182 21 Prague 8, Czech Republic
³⁰Iowa State University, Ames, Iowa 50011, USA
³¹Advanced Science Research Center, Japan Atomic Energy Agency, 2-4 Shirakata Shirane, Tokai-mura, Naka-gun, Ibaraki-ken 319-1195, Japan
³²Joint Institute for Nuclear Research, 141980 Dubna, Moscow Region, Russia
³³Helsinki Institute of Physics and University of Jyväskylä, P.O.Box 35, FI-40014 Jyväskylä, Finland
³⁴Károly Róberts University College, H-3200 Gyöngyös, Mátraiút 36, Hungary
³⁵KEK, High Energy Accelerator Research Organization, Tsukuba, Ibaraki 305-0801, Japan
³⁶Korea University, Seoul, 136-701, Korea
³⁷National Research Center “Kurchatov Institute”, Moscow, 123098 Russia
³⁸Kyoto University, Kyoto 606-8502, Japan
³⁹Laboratoire Leprince-Ringuet, Ecole Polytechnique, CNRS-IN2P3, Route de Saclay, F-91128, Palaiseau, France
⁴⁰Physics Department, Lahore University of Management Sciences, Lahore 54792, Pakistan
⁴¹Lawrence Livermore National Laboratory, Livermore, California 94550, USA
⁴²Los Alamos National Laboratory, Los Alamos, New Mexico 87545, USA
⁴³LPC, Université Blaise Pascal, CNRS-IN2P3, Clermont-Fd, 63177 Aubiere Cedex, France
⁴⁴Department of Physics, Lund University, Box 118, SE-221 00 Lund, Sweden
⁴⁵University of Maryland, College Park, Maryland 20742, USA
⁴⁶Department of Physics, University of Massachusetts, Amherst, Massachusetts 01003-9337, USA
⁴⁷Department of Physics, University of Michigan, Ann Arbor, Michigan 48109-1040, USA
⁴⁸Institut für Kernphysik, University of Muenster, D-48149 Muenster, Germany
⁴⁹Muhlenberg College, Allentown, Pennsylvania 18104-5586, USA
⁵⁰Myongji University, Yongin, Kyonggido 449-728, Korea
⁵¹Nagasaki Institute of Applied Science, Nagasaki-shi, Nagasaki 851-0193, Japan
⁵²Nara Women’s University, Kita-uoya Nishi-machi Nara 630-8506, Japan
⁵³National Research Nuclear University, MEPhI, Moscow Engineering Physics Institute, Moscow, 115409, Russia
⁵⁴University of New Mexico, Albuquerque, New Mexico 87131, USA
⁵⁵New Mexico State University, Las Cruces, New Mexico 88003, USA
⁵⁶Department of Physics and Astronomy, Ohio University, Athens, Ohio 45701, USA
⁵⁷Oak Ridge National Laboratory, Oak Ridge, Tennessee 37831, USA
⁵⁸IPN-Orsay, Univ. Paris-Sud, CNRS/IN2P3, Université Paris-Saclay, BP1, F-91406, Orsay, France
⁵⁹Peking University, Beijing 100871, P. R. China
⁶⁰PNPI, Petersburg Nuclear Physics Institute, Gatchina, Leningrad region, 188300, Russia
⁶¹RIKEN Nishina Center for Accelerator-Based Science, Wako, Saitama 351-0198, Japan
⁶²RIKEN BNL Research Center, Brookhaven National Laboratory, Upton, New York 11973-5000, USA
⁶³Physics Department, Rikkyo University, 3-34-1 Nishi-Ikebukuro, Toshima, Tokyo 171-8501, Japan
⁶⁴Saint Petersburg State Polytechnic University, St. Petersburg, 195251 Russia
⁶⁵Universidade de São Paulo, Instituto de Física, Caixa Postal 66318, São Paulo CEP05315-970, Brazil
⁶⁶Department of Physics and Astronomy, Seoul National University, Seoul 151-742, Korea
⁶⁷Chemistry Department, Stony Brook University, SUNY, Stony Brook, New York 11794-3400, USA
⁶⁸Department of Physics and Astronomy, Stony Brook University, SUNY, Stony Brook, New York 11794-3800, USA
⁶⁹SUBATECH (Ecole des Mines de Nantes, CNRS-IN2P3, Université de Nantes) BP 20722-44307, Nantes, France
⁷⁰University of Tennessee, Knoxville, Tennessee 37996, USA
⁷¹Department of Physics, Tokyo Institute of Technology, Oh-okayama, Meguro, Tokyo 152-8551, Japan
⁷²Center for Integrated Research in Fundamental Science and Engineering, University of Tsukuba, Tsukuba, Ibaraki 305, Japan
⁷³Vanderbilt University, Nashville, Tennessee 37235, USA
⁷⁴Waseda University, Advanced Research Institute for Science and Engineering, 17 Kikui-cho, Shinjuku-ku, Tokyo 162-0044, Japan
⁷⁵Weizmann Institute, Rehovot 76100, Israel
⁷⁶Institute for Particle and Nuclear Physics, Wigner Research Centre for Physics, Hungarian Academy of Sciences (Wigner RCP, RMKI) H-1525 Budapest 114, POBox 49, Budapest, Hungary
⁷⁷Yonsei University, IPAP, Seoul 120-749, Korea
⁷⁸University of Zagreb, Faculty of Science, Department of Physics, Bijenička 32, HR-10002 Zagreb, Croatia

(Dated: December 3, 2015)

Measurements of the fractional momentum loss ($S_{\text{loss}} \equiv \delta p_T/p_T$) of high-transverse-momentum-identified hadrons in heavy ion collisions are presented. Using π^0 in Au+Au and Cu+Cu collisions at $\sqrt{s_{NN}} = 62.4$ and 200 GeV measured by the PHENIX experiment at the Relativistic Heavy Ion Collider and charged hadrons in Pb+Pb collisions measured by the ALICE experiment at the Large Hadron Collider, we studied the scaling properties of S_{loss} as a function of a number of variables: the number of participants, N_{part} , the number of quark participants, N_{qp} , the charged-particle density, $dN_{\text{ch}}/d\eta$, and the Bjorken energy density times the equilibration time, $\varepsilon_{\text{Bj}}\tau_0$. We find that the p_T , where S_{loss} has its maximum, varies both with centrality and collision energy. Above the maximum, S_{loss} tends to follow a power-law function with all four scaling variables. The data at $\sqrt{s_{NN}} = 200$ GeV and 2.76 TeV, for sufficiently high particle densities, have a common scaling of S_{loss} with $dN_{\text{ch}}/d\eta$ and $\varepsilon_{\text{Bj}}\tau_0$, lending insight on the physics of parton energy loss.

PACS numbers: 25.75.Dw

I. INTRODUCTION

It has been firmly established that in relativistic heavy ion collisions a hot, dense medium is rapidly formed, capable of interacting with the high p_T partons produced in primordial hard scattering and making them lose some energy while traversing the medium [1–4]. Such energy loss in the medium was first predicted in early 1980’s [5]. Quantifying this energy loss is an important issue, because it is directly connected to the properties of the medium. However, this is not straightforward since neither the original parton energy, nor that of the decelerated one is easily accessible. Back-to-back photon-jet pairs in principle give access to both the initial and final parton energy, but such events are rare, because they are suppressed by a factor $\alpha_{em}\alpha_s$, the electromagnetic coupling constant. Measurement of jets give more complete information on the parton energy loss, however, their measurement is challenging, particularly at high multiplicities and low parton p_T . To circumvent this, high p_T hadrons are often used as proxies for jets (“leading hadrons”), and the parton energy loss in principle can be calculated by proper comparison of the invariant yields of hadrons in $p+p$ and $A+A$ at a given p_T . For this purpose the $p+p$ yields are usually scaled up by the expected number of binary nucleon-nucleon collisions in $A+A$, estimated from a Glauber Monte-Carlo model, and in the absence of any initial or final state nuclear effects they are expected to coincide with the $A+A$ yields. The partons have steeply falling momentum spectra, so if partons lose energy, that results in a shift of the momentum spectra, and the yield at a given p_T will become suppressed [6]. Utilizing this fact, the nuclear-modification factor (R_{AA}) has become a widely used characterization of the energy loss which is defined as:

$$R_{AA}(p_T) = \frac{(1/N_{AA}^{\text{evt}})d^2N_{AA}^h/dp_T dy}{\langle T_{AA} \rangle \times d^2\sigma_{pp}^h/dp_T dy}, \quad (1)$$

where σ_{pp}^h is the production cross section of the respective hadron in $p+p$ collisions, $\langle T_{AA} \rangle = \langle N_{\text{coll}} \rangle / \sigma_{pp}^{\text{inel}}$ is the nuclear overlap function averaged over the relevant range of impact parameters, and $\langle N_{\text{coll}} \rangle$ is the number of binary nucleon-nucleon collisions computed with $\sigma_{pp}^{\text{inel}}$. If R_{AA} is unity, it is usually assumed that the yield measured in $A+A$ collisions is explained by the primordial hard production as observed in $p+p$ collisions with no nuclear or medium effect. If $R_{AA} < 1$ (suppression) the $A+A$ yield at a given p_T is less than that expected from the scaled $p+p$.

While the parton energy loss is expected to depend both on system size and collision energy, it is remarkable that R_{AA} is very similar from $\sqrt{s_{NN}} = 62.4$ to 200 GeV at the Relativistic Heavy Ion Collider (RHIC) and up to 2.76 TeV at the Large Hadron Collider (LHC). The reason is that while the energy loss increases with increasing $\sqrt{s_{NN}}$ which would tend to decrease R_{AA} , the power n in the p_T^{-n} shaped spectra decreases ($n = 10.6$ for 62.4 GeV [7], $n = 8.06$ for 200 GeV Au+Au and $n \approx 6.0$ for 2.76 TeV [8]) and provides a countervailing effect. A numerical calculation showed that the fractional energy loss of partons, $\Delta E/E$, is indeed significantly different between LHC and RHIC even though the R_{AA} is similar [9].

Instead of R_{AA} one can employ the fractional momentum loss (S_{loss}) of high p_T hadrons as a measure of parton energy loss which should reflect the average fractional energy loss of the initial partons ($\langle \Delta E/E \rangle \sim S_{\text{loss}}$). S_{loss} is defined as

$$S_{\text{loss}} \equiv \delta p_T/p_T = \frac{p_T^{pp} - p_T^{AA}}{p_T^{pp}} \quad (2)$$

where p_T^{AA} is the p_T of the $A+A$ measurement and p_T^{pp} is that of the $p+p$ measurement scaled by the nuclear overlap function T_{AA} of the corresponding $A+A$ centrality class at the same yield of the $A+A$ measurement. We calculate S_{loss} as a function of the original momentum of partons that are represented by p_T^{pp} .

Under the assumptions that N_{coll} scaling is applicable and fragmentation functions are unchanged from $p+p$ collisions, δp_T can be directly measured as the shift in p_T needed to get the same yield ($dN/dp_T dy$) in $A+A$ as the scaled $p+p$.

* Deceased

† PHENIX Co-Spokesperson: morrison@bnl.gov

‡ PHENIX Co-Spokesperson: jamie.nagle@colorado.edu

The PHENIX experiment published a study of the energy loss of partons by converting azimuthal angle (ϕ)-dependent R_{AA} with respect to the event plane to S_{loss} assuming that the spectra follow a power-law function [10]. That study found that S_{loss} scales with L_ϵ , the distance from the center to the edge of the collision area which the partons traverse, for all centrality classes for $3 < p_T < 8$ GeV/c, and also with the density-weighted path length $\rho L / \rho_{\text{cent}}$ where ρ_{cent} is the density at the center of the collision zone and the ρ is the density at the given coordinate. The dependence of S_{loss} on centrality was also reasonably approximated by $N_{\text{part}}^{2/3}$. A similar study has been performed using Pb+Pb data available at LHC and Au+Au data from RHIC [11]. The authors found that the scaling in [10] does not hold at p_T higher than 10 GeV/c. Other recent publications tried to obtain ϕ -integrated S_{loss} without assuming the spectral shape [7, 8]. It was found that S_{loss} varies by a factor of six from 62.4 GeV Au+Au to 2.76 TeV Pb+Pb collisions. These studies showed that the fractional momentum loss S_{loss} has a major advantage over R_{AA} , in that it allows for a direct comparison of parton energy loss between different colliding systems and energies, because it eliminates the bias owing to the $\sqrt{s_{NN}}$ -variation of the exponent, n , in the power-law spectra of high p_T particles.

These scaling studies are not a replacement for full quantum-chromodynamics calculations of parton energy loss that must include different quark and gluon admixtures and their different fragmentation functions, initial state effects such as nuclear modified parton distribution functions, and potentially modified harmonization effects. That said, since S_{loss} is merely a new representation of the experimental measurements, any such theoretical calculation would need to describe the observed scalings at the precision of the uncertainties.

In this paper, we extend the previous studies of ϕ -integrated S_{loss} by including additional data sets both from RHIC and LHC and by plotting the fractional momentum loss against several scaling variables to characterize the energy loss mechanism. We average over the event plane dependence to simplify the analysis. Section II describes the method of calculating S_{loss} and introduces the global scaling variables. In section III A, we present values for S_{loss} as a function of centrality for a variety of systems and energies. Section III B presents the main result of this paper, which is the study of the scaling behavior of S_{loss} . We conclude in section IV.

II. DATASET AND ANALYSIS

In this section we describe how fractional momentum loss is calculated and define the various scaling variables. A summary of the data is given in Table I. The numerical values of the scaling variables are listed in Table III. For RHIC energies, data from the PHENIX experiment for π^0 in Au+Au and Cu+Cu collisions both

TABLE I. Summary of data sets used in this analysis. The $\sqrt{s_{NN}} = 62.4$ and 200 GeV data are from PHENIX at RHIC and the $\sqrt{s_{NN}} = 2.76$ TeV data from ALICE at the LHC.

System	particle	$\sqrt{s_{NN}}$	year	p_T range	ref.
Au+Au	π^0	200 GeV	2004	1.0–20 GeV/c	[12]
Au+Au	π^0	200 GeV	2007	5.0–20 GeV/c	[8]
Cu+Cu	π^0	200 GeV	2005	1.0–18 GeV/c	[13]
$p+p$ $\overline{p}+\overline{p}$	π^0	200 GeV	2005	0.5–20 GeV/c	[14]
Au+Au	π^0	62.4 GeV	2010	1.0–10 GeV/c	[7]
Cu+Cu	π^0	62.4 GeV	2005	1.0–8.0 GeV/c	[13]
$p+p$ $\overline{p}+\overline{p}$	π^0	62.4 GeV	2006	0.5–7.0 GeV/c	[15]
Pb+Pb	$h^{+/-}$	2.76 TeV	2010	0.2–50 GeV/c	[16]
Pb+Pb	$\pi^{+/-}$	2.76 TeV	2010–2011	2.0–20 GeV/c	[17]
Pb+Pb	π^0	2.76 TeV	2010	0.5–11 GeV/c	[18]
$p+p$ $\overline{p}+\overline{p}$	$h^{+/-}$	2.76 TeV	2009–2011	0.2–50 GeV/c	[19]
$p+p$ $\overline{p}+\overline{p}$	$\pi^{+/-}$	2.76 TeV	2010–2011	2.0–20 GeV/c	[17]
$p+p$ $\overline{p}+\overline{p}$	π^0	2.76 TeV	2011	0.5–11 GeV/c	[18]

at $\sqrt{s_{NN}} = 200$ GeV and 62.4 GeV were used [7, 8, 12–15], while for the LHC, data on charged hadrons and pions in Pb+Pb collisions, both at $\sqrt{s_{NN}} = 2.76$ TeV, measured by the ALICE experiment [16–19] were used. To calculate the fractional momentum loss, $p+p$ data are also needed: RHIC data were taken from [14, 15], while LHC data were taken from [19].

~~Global variables for Au+Au and Cu+Cu collisions at RHIC from PHENIX and Pb+Pb collisions at the LHC from ALICE. Collision Centrality GeV/fm² Au+Au 200 GeV 0 5353±10.0 957±16.2 687±37.0 5.42±0.59 0 10327±9.5 873±15.8 624±32.4 5.17±0.56 10 20235±7.7 597±13.4 415±20.0 4.28±0.47 20 30166±6.3 403±11.3 274±15.1 3.48±0.40 30 40114±5.3 263±10.1 177±11.6 2.74±0.34 40 5075.0±4.5 162±6.1 110±9.2 2.06±0.28 50 6046.4±4.0 91.5±6.2 61.6±7.1 1.38±0.23 60 7026.1±3.5 51.3±6.9 31.6±5.0 0.83±0.18 Cu+Cu 200 GeV 0 1096.9±3.9 238±12.2 178±14.2 3.00±0.36 10 2074.3±3.9 175±10.5 123±9.9 2.43±0.27 20 3053.7±2.7 121±8.7 85.0±6.8 2.00±0.25 30 4039.9±3.8 87.1±9.0 57.7±4.6 1.58±0.19 40 5028.1±3.3 59.0±7.9 38.2±3.0 1.24±0.17 Au+Au 62.4 GeV 0 10317±6.1 824±21.0 405±32.4 3.41±0.36 10 20225±9.3 560±17.4 273±20.9 2.95±0.30 20 40131±8.5 310±12.9 151±13.1 2.17±0.22 40 6054.7±6.0 118±8.0 57.5±4.3 1.31±0.13 Cu+Cu 62.4 GeV 0 1095.9±2.1 222±9.1 122±8.9 1.98±0.22 10 2073.7±2.6 164±8.4 84.5±6.5 1.65±0.19 20 3055.2±2.5 118±7.0 58.0±4.5 1.35±0.16 30 4040.5±2.4 83.6±6.7 39.0±3.0 1.10±0.13 40 5028.2±2.2 56.0±5.1 25.5±2.0 0.89±0.11 Pb+Pb 2.76 TeV 0 5383±3.1 1086±14.1~~

1601±60 11.5±1.43 5 10330±4.6 915±11.9 1294±49
 10.5±1.27 10 20261±4.4 706±10.6 966±37 9.05±1.41
 20 30186±3.9 488±8.3 649±23 7.35±1.21 30 40129±3.3
 325±7.5 426±15 5.99±0.91 40 5085.0±2.6 205±5.9
 261±9 4.69±0.75 50 6052.8±2.0 118±3.5 149±6
 3.47±0.49 60 7030.0±1.3 60.9±2.0 76±4 2.11±0.35
 70 8015.8±0.6 26.3±0.9 35±2 1.17±0.22

A. Fractional momentum loss

Figure 1 shows the method of calculating the S_{loss} using measured A+A and $p+p$ spectra at the same collision energy. First, the π^0 ($\pi^{+/-}$, $h^{+/-}$) cross section in $p+p$ is scaled by T_{AA} corresponding to the centrality selection of the A+A data. Second, the scaled $p+p$ cross section is fit with a power-law function. Third, the scaled $p+p$ point, p_T^{pp} , corresponding to the yield at the Au+Au point of interest, is found using the fit to interpolate between scaled $p+p$ points. The δp_T is calculated as $p_T^{pp} - p_T^{AA}$. To obtain S_{loss} , the δp_T is divided by p_T^{pp} .

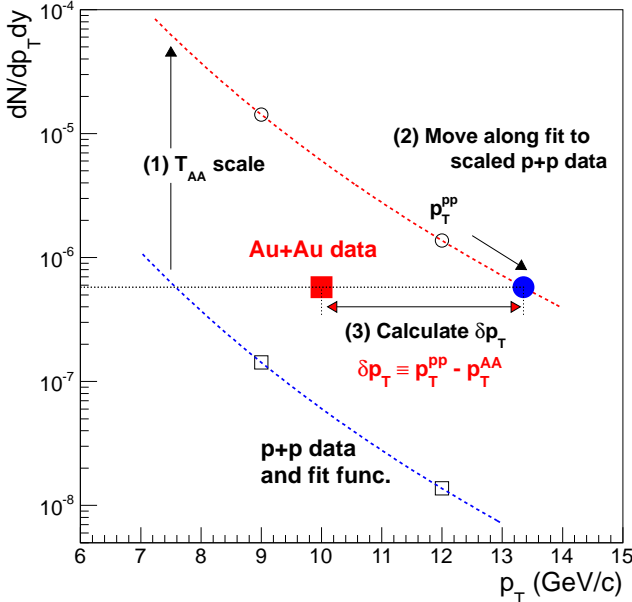


FIG. 1. (Color online) Method of calculating the fractional momentum loss ($S_{\text{loss}} \equiv \delta p_T / p_T$). This plot is for illustration only; uncertainties are not shown. The procedure: (1) scale the $p+p$ data by T_{AA} corresponding to the centrality selection of A+A data, (2) fit the $p+p$ data and choose the scaled $p+p$ point closest in yield to the A+A along the fit, (3) calculate the difference of scaled $p+p$ and A+A transverse momenta, $\delta p_T \equiv p_T^{pp} - p_T^{AA}$, at the same yield.

It is important to realize that the effective fractional energy loss, S_{loss} , estimated from the shift in the p_T spectrum, is actually less than the real average energy loss at a given p_T . This is true because, for a given observed p_T^{AA} , the events at much larger p_T with larger energy loss are lost under the events at smaller p_T with a corre-

spondingly smaller energy loss owing to the steeply falling spectrum. We evaluated this bias to the S_{loss} measurement with a simple Monte Carlo calculation using the power of the spectra obtained in the measurements, and found that it is $\sim 10\%$ for collisions at $\sqrt{s_{NN}} = 200$ GeV and 62.4 GeV, and $\sim 18\%$ for $\sqrt{s_{NN}} = 2.76$ TeV. This systematic effect is not reflected in the final data uncertainties.

The uncertainties of the S_{loss} are obtained as follows. We first estimated the errors of yields for the A+A and the $p+p$ points in three categories; the quadratic sum of the statistical and p_T -independent systematic uncertainties (“Type A”), p_T -correlated systematic uncertainties (“Type B”), and the overall scale uncertainties which allow all the data points to move to the same direction with a certain fraction of the central values (“Type C”). The Type B is the quadratic sum of the systematic uncertainties related to the measurement of π^0 for the PHENIX result, including those of photon identification efficiency, energy scale, and background subtraction. The Type C is the quadratic sum of the T_{AA} and $p+p$ normalization uncertainties in this analysis. The uncertainties for the A+A and $p+p$ points in three categories are separately summed in quadrature, and projected to the p_T^{pp} axis using the $p+p$ fit function.

B. Number of Nucleon and Quark Participants

To study the systematics of fractional momentum loss, we introduce several scaling variables. Here we briefly describe how the number of nucleon participants (N_{part}) and quark participants (N_{qp}) [20] are obtained. The N_{part} for the Pb+Pb collisions at $\sqrt{s_{NN}} = 2.76$ TeV was taken from [21]. The number of quark-participants is calculated for all systems as part of this work, as explained below.

A Monte-Carlo-Glauber (MC-Glauber) model calculation [22] is used to obtain estimates for the number of nucleon participants at each centrality using the procedure described in [23]. A similar procedure can be used to estimate the number of quark participants, N_{qp} , at each centrality [20]. The MC-Glauber calculation is modified such that the fundamental interactions are quark-quark rather than nucleon-nucleon collisions. The nuclei are assembled by distributing the centers of the nucleons according to a Woods-Saxon distribution. Once a nucleus is assembled, three quarks are then distributed around the center of each nucleon. In our model, we assume the spatial distribution of the quarks follows an exponential charge distribution as measured in electron-proton elastic scattering:

$$\rho^{\text{proton}}(r) = \rho_0^{\text{proton}} \times e^{-ar}, \quad (3)$$

where $a = \sqrt{12}/r_m = 4.27 \text{ fm}^{-1}$ and $r_m = 0.81 \text{ fm}$ is the rms charge radius of the proton [24]. The coordinates of the two colliding nuclei are shifted at random relative to each other by a vector \vec{b} , the impact parameter, which

covers an area larger than the maximum possible impact parameter. A pair of quarks, one from each nucleus, interact with each other if their distance d in the plane transverse to the beam axis satisfies the condition

$$d < \sqrt{\frac{\sigma_{qq}^{\text{inel}}}{\pi}}, \quad (4)$$

where $\sigma_{qq}^{\text{inel}}$ is the inelastic quark-quark cross section, which is varied for the case of nucleon-nucleon collisions until the known inelastic nucleon-nucleon cross section is reproduced; this $\sigma_{qq}^{\text{inel}}$ is then used for the A+A calculations. The inelastic quark-quark cross sections are tabulated in Table II. Figure 2a shows the number of quark participants as a function of the number of nucleon participants [20]. The relationship is nonlinear, especially for low values of N_{part} . The nonlinearity is clearly seen in Fig. 2b where the ratio of the number of quark participants to the number of nucleon participants as a function of the number of nucleon participants is shown.

TABLE II. The inelastic quark-quark cross sections used for each collision energy to reproduce the inelastic nucleon-nucleon cross section.

$\sqrt{s_{NN}}$ (GeV)	$\sigma_{NN}^{\text{inel}}$ (mb)	$\sigma_{qq}^{\text{inel}}$ (mb)
2760	64.0	18.4
200	42.3	9.36
62.4	36.0	7.08

C. Charged Particle Multiplicity

Another scaling variable used is charged particle multiplicity, or multiplicity density, $dN_{\text{ch}}/d\eta$, measured at midrapidity ($y \approx \eta \approx 0$). This quantity is closely related to the gluon density, dN_{gluon}/dy [25], as well as to the number of participating nucleons N_{part} , which in turn is a measure of the system size. In a previous publication [23] it has been shown that

$$dN_{\text{ch}}/d\eta \propto N_{\text{part}}^{\alpha} \quad (5)$$

where $\alpha=1.16$ in Au+Au collisions at $\sqrt{s_{NN}} = 200$ GeV. For the RHIC data $dN_{\text{ch}}/d\eta$ values were taken from the PHENIX experiment [20, 23], where charged particle multiplicities are measured in the $|\eta| < 0.35$ pseudorapidity region in two pad chamber detectors [26] in zero magnetic field. For the LHC data $dN_{\text{ch}}/d\eta$, values are quoted from the ALICE publication [21], where charged particles are measured in their silicon-pixel detector and quoted in the restricted $|\eta| < 0.5$ pseudorapidity range.

D. Bjorken Energy Density

Finally, we introduce a measure of the energy density. In relativistic heavy ion collisions, the Bjorken energy

density is frequently used for this purpose [27]. The Bjorken energy density is defined as

$$\epsilon_{Bj} = \frac{1}{\tau_0 A_{\perp}} \frac{dE_T}{dy} \quad (6)$$

where τ_0 is the proper time when the QGP is equilibrated, A_{\perp} is the transverse area of the system. The A_{\perp} can be written as $\sim \sigma_x \sigma_y$, where σ_x and σ_y are the widths of x and y position distributions of the participating nucleons in the transverse plane, and was estimated using a Monte-Carlo Glauber simulation [22]. The equilibration time τ_0 is strongly model-dependent, therefore, we decided to use $\epsilon_{Bj} \tau_0$ as a scaling variable, which then contains only well-established experimental quantities. The measured $dE_T/d\eta$ is converted to dE_T/dy by applying a factor that compensates the phase space difference between rapidity and pseudorapidity which is obtained by a simple numerical calculation. The factor is found to be 1.25 for $\sqrt{s_{NN}} = 62.4$ GeV and $\sqrt{s_{NN}} = 200$ GeV [23], and 1.09 for $\sqrt{s_{NN}} = 2.76$ TeV [28]. The uncertainties on these scale numbers are $\sim 3\%$. The $dE_T/d\eta$ for the $\sqrt{s_{NN}} = 2.76$ TeV Pb+Pb collisions are obtained from the literature [29].

III. RESULTS AND DISCUSSION

The numerical values of the scaling variables introduced in the previous section are listed in Table III.

A. p_T dependence of the fractional momentum loss

Figure 3 shows the p_T dependence of the fractional momentum loss of π^0 for various centralities in Au+Au 200 GeV collisions, using 2007 data [8]. The error bars represent the projection of Type A uncertainties to the p_T^{pp} axis, while the boxes are the same projection of Type B uncertainties. $\delta_{\text{sys}}(T_{AA} \oplus \text{pp norm})$ shown in the following plots stands for the projection of Type C uncertainties to the p_T^{pp} axis. Note that $\delta_{\text{sys}}(T_{AA} \oplus \text{pp norm})$ indicate the absolute amount that the data points would move.

The 2007 data set has been analyzed only above $p_T = 5$ GeV/c, which also limits the p_T where S_{loss} can be extracted. For lower p_T the 2004 data were used [12], and the results are shown in open symbols in Fig. 3. The consistency of R_{AA} from 2004 and 2007 data has already been shown in Fig. 11 of [12]. The same consistency can be seen in the extracted S_{loss} . In the central collisions S_{loss} is slightly increasing up to ~ 6 GeV/c, then flattens out and finally decreases at the highest measured p_T . As expected, S_{loss} increases monotonically with centrality.

We show the fractional momentum loss of π^0 for various centralities in Cu+Cu 200 GeV collisions in Fig. 4.

We already found in a previous publication that R_{AA} is similar at the same N_{part} between Cu+Cu and Au+Au

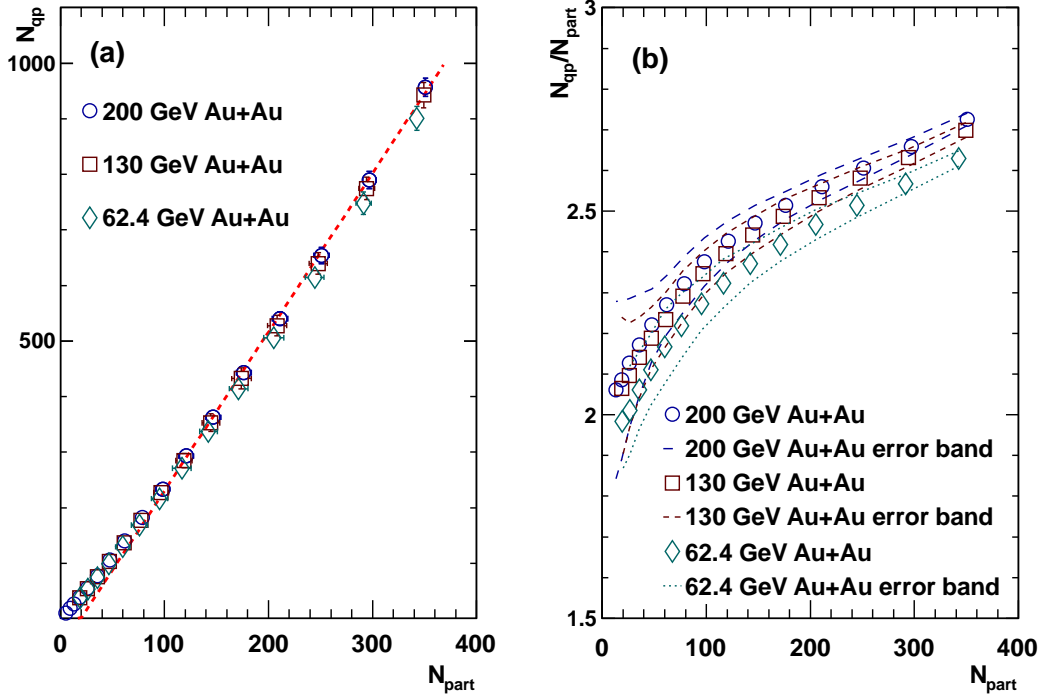


FIG. 2. (Color online) (a) The number of quark participants as a function of the number of nucleon participants. The error bars represent the systematic uncertainty estimate on the MC-Glauber calculation. The dashed line is a linear fit to the 200 GeV Au+Au points with $N_{part} > 100$ to illustrate the nonlinearity of the correlation at low values of N_{part} . (b) The ratio of the number of quark participants to the number of nucleon participants as a function of the number of nucleon participants. The error bands represent the systematic uncertainty estimate on the MC-Glauber calculation. This figure is reproduced from [20].

collisions at $\sqrt{s_{NN}} = 200$ GeV [13]. The N_{part} for 0%–10% centrality in Cu+Cu collisions is similar to the one for 30%–40% centrality in Au+Au collisions. We can see that the S_{loss} is similar in these collision from Figs. 3 and 4.

The fraction of hard-scattering is smaller and therefore results in a steeper p_T spectrum at $\sqrt{s_{NN}} = 62.4$ GeV. Figure 5 shows the fractional momentum loss of π^0 for various centralities in Au+Au 62.4 GeV collisions.

The S_{loss} is much smaller than at 200 GeV even for the most central collisions. Note that soft production in $A + A$ collisions still contributes to the p_T^p range of 2–6 GeV/c, where R_{AA} is not reaching to its minimum [7]. In the S_{loss} , this will result in smaller values. Figure 6 shows the S_{loss} of π^0 for various centralities in 62.4 GeV Cu+Cu collisions [7].

The trends are similar for the Cu+Cu and Au+Au collision data. Note that in the 62.4 GeV data set the systematic uncertainties from π^0 reconstruction, overall energy scale and trigger efficiency were larger [13] than in the 200 GeV Au+Au data, which explains the larger overall systematic uncertainties. It is again interesting to mention that within the uncertainties, the 0%–10% Cu+Cu collisions give the similar S_{loss} as the 20%–40% Au+Au collisions even at this energy.

In Fig. 7, we show the fractional momentum loss for charged hadrons in Pb+Pb collisions at $\sqrt{s_{NN}} = 2.76$ TeV measured by the ALICE experiment [16, 19].

A clear increase of the S_{loss} is seen in the 4–10 GeV/c region with the maximum being dependent on centrality. Despite the $\approx 10\%$ –fold difference of $\sqrt{s_{NN}}$ between RHIC and LHC, the trend is rather consistent, but more pronounced at the LHC and without a region of constant S_{loss} as is most evident in the PHENIX 0%–10% data in Fig. 3.

The ALICE experiment recently published the spectra for charged pions for two centrality classes [17]. We computed the fractional momentum loss for charged pions and compared with those for charged hadrons as shown in Fig. 8. For peripheral collisions, we plot the results for charged hadrons in 60%–70% and 70%–80% bins. For 0%–5% centrality, the S_{loss} for charged hadrons are systematically lower than that of charged pions at $p_T < 10$ GeV/c, and both of them become similar above 10 GeV/c. This observation is consistent with the enhanced baryon production in $p_T < 10$ GeV/c compared to mesons in the central collisions [17]. Charged hadron spectra include protons, and thus the suppression is smaller for them in the medium p_T region. In the 60%–80% centrality, the charged pions and charged hadrons

TABLE III. Global variables for Au+Au and Cu+Cu collisions at RHIC from PHENIX [7, 8, 12, 13] and Pb+Pb collisions at the LHC from ALICE [16, 17, 30].

<u>Collision</u>	<u>$\sqrt{s_{NN}}$</u>	<u>Centrality</u>	<u>N_{part}</u>	<u>N_{qp}</u>	<u>$dN_{\text{ch}}/d\eta$</u>	<u>$\varepsilon_{\text{Bj}}\tau_0$ [GeV/fm²]</u>
<u>Au+Au</u>	<u>200 GeV</u>	<u>0%–5%</u>	<u>353±10.0</u>	<u>957±16.2</u>	<u>687±37.0</u>	<u>5.42±0.59</u>
		<u>0%–10%</u>	<u>327±9.5</u>	<u>873±15.8</u>	<u>624±32.4</u>	<u>5.17±0.56</u>
		<u>10%–20%</u>	<u>235±7.7</u>	<u>597±13.4</u>	<u>415±20.0</u>	<u>4.28±0.47</u>
		<u>20%–30%</u>	<u>166±6.3</u>	<u>403±11.3</u>	<u>274±15.1</u>	<u>3.48±0.40</u>
		<u>30%–40%</u>	<u>114±5.3</u>	<u>263±10.1</u>	<u>177±11.6</u>	<u>2.74±0.34</u>
		<u>40%–50%</u>	<u>75.0±4.5</u>	<u>162±6.1</u>	<u>110±9.2</u>	<u>2.06±0.28</u>
		<u>50%–60%</u>	<u>46.4±4.0</u>	<u>91.5±6.2</u>	<u>61.6±7.1</u>	<u>1.38±0.23</u>
		<u>60%–70%</u>	<u>26.1±3.5</u>	<u>51.3±6.9</u>	<u>31.6±5.0</u>	<u>0.83±0.18</u>
<u>Cu+Cu</u>	<u>200 GeV</u>	<u>0%–10%</u>	<u>96.9±3.9</u>	<u>238±12.2</u>	<u>178±14.2</u>	<u>3.00±0.36</u>
		<u>10%–20%</u>	<u>74.3±3.9</u>	<u>175±10.5</u>	<u>123±9.9</u>	<u>2.43±0.27</u>
		<u>20%–30%</u>	<u>53.7±2.7</u>	<u>121±8.7</u>	<u>85.0±6.8</u>	<u>2.00±0.25</u>
		<u>30%–40%</u>	<u>39.9±3.8</u>	<u>87.1±9.0</u>	<u>57.7±4.6</u>	<u>1.58±0.19</u>
		<u>40%–50%</u>	<u>28.1±3.3</u>	<u>59.0±7.9</u>	<u>38.2±3.0</u>	<u>1.24±0.17</u>
<u>Au+Au</u>	<u>62.4 GeV</u>	<u>0%–10%</u>	<u>317±6.1</u>	<u>824±21.0</u>	<u>405±32.4</u>	<u>3.41±0.36</u>
		<u>10%–20%</u>	<u>225±9.3</u>	<u>560±17.4</u>	<u>273±20.9</u>	<u>2.95±0.30</u>
		<u>20%–40%</u>	<u>131±8.5</u>	<u>310±12.9</u>	<u>151±13.1</u>	<u>2.17±0.22</u>
		<u>40%–60%</u>	<u>54.7±6.0</u>	<u>118±8.0</u>	<u>57.5±4.3</u>	<u>1.31±0.13</u>
<u>Cu+Cu</u>	<u>62.4 GeV</u>	<u>0%–10%</u>	<u>95.9±2.1</u>	<u>222±9.1</u>	<u>122±8.9</u>	<u>1.98±0.22</u>
		<u>10%–20%</u>	<u>73.7±2.6</u>	<u>164±8.4</u>	<u>84.5±6.5</u>	<u>1.65±0.19</u>
		<u>20%–30%</u>	<u>55.2±2.5</u>	<u>118±7.0</u>	<u>58.0±4.5</u>	<u>1.35±0.16</u>
		<u>30%–40%</u>	<u>40.5±2.4</u>	<u>83.6±6.7</u>	<u>39.0±3.0</u>	<u>1.10±0.13</u>
		<u>40%–50%</u>	<u>28.2±2.2</u>	<u>56.0±5.1</u>	<u>25.5±2.0</u>	<u>0.89±0.11</u>
<u>Pb+Pb</u>	<u>2.76 TeV</u>	<u>0%–5%</u>	<u>383±3.1</u>	<u>1086±14.1</u>	<u>1601±60</u>	<u>11.5±1.43</u>
		<u>5%–10%</u>	<u>330±4.6</u>	<u>915±11.9</u>	<u>1294±49</u>	<u>10.5±1.27</u>
		<u>10%–20%</u>	<u>261±4.4</u>	<u>706±10.6</u>	<u>966±37</u>	<u>9.05±1.41</u>
		<u>20%–30%</u>	<u>186±3.9</u>	<u>488±8.3</u>	<u>649±23</u>	<u>7.35±1.21</u>
		<u>30%–40%</u>	<u>129±3.3</u>	<u>325±7.5</u>	<u>426±15</u>	<u>5.99±0.91</u>
		<u>40%–50%</u>	<u>85.0±2.6</u>	<u>205±5.9</u>	<u>261±9</u>	<u>4.69±0.75</u>
		<u>50%–60%</u>	<u>52.8±2.0</u>	<u>118±3.5</u>	<u>149±6</u>	<u>3.47±0.49</u>
		<u>60%–70%</u>	<u>30.0±1.3</u>	<u>60.9±2.0</u>	<u>76±4</u>	<u>2.11±0.35</u>
		<u>70%–80%</u>	<u>15.8±0.6</u>	<u>26.3±0.9</u>	<u>35±2</u>	<u>1.17±0.22</u>

give similar results. This feature is again consistent with the observation of enhanced baryon production both at RHIC and LHC which only occurs in the central collisions. The ALICE experiment also published neutral pion data very recently, from which we calculated the S_{loss} for the data set as shown in Figure 9 [18].

The neutral pion results have finer centrality selections, but have a limited p_T range and larger uncertainties, therefore, they were not considered in further studies of scaling variable dependence. We can see that the S_{loss} for neutral pions are similar to that of charged pions and hence are consistent with charged hadrons for $p_T > 10$ GeV/ c .

B. Scaling variable dependence

To understand how the fractional momentum loss changes with collision systems, we plot S_{loss} against the scaling variables defined in the section II. Figures 10 and 11 show the S_{loss} as a function of N_{part} , N_{qp} , $dN_{\text{ch}}/d\eta$, and $\varepsilon_{\text{Bj}}\tau_0$ at $p_T^{pp} = 7$ and 12 GeV/ c , respec-

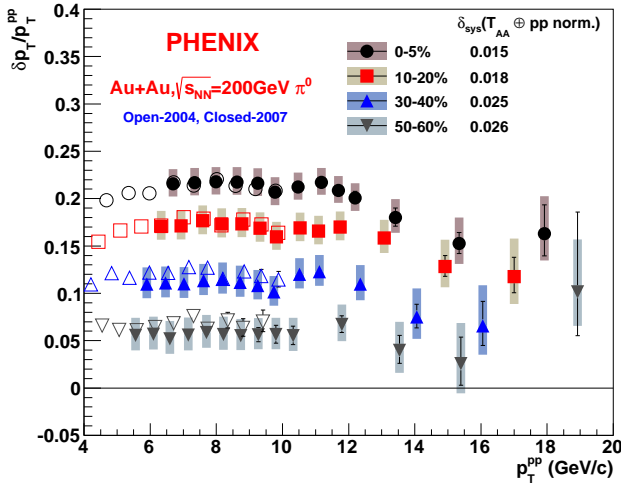


FIG. 3. (Color online) p_T^{pp} dependence of S_{loss} for π^0 in 200 GeV Au+Au collisions from (solid symbols) 2007 data [8] and (open symbols) 2004 data from the PHENIX experiment at RHIC for $p_T < 10$ GeV/c [12]. The error boxes corresponding to Type-B errors are not shown for Year-2004 data, but the magnitude are same as the ones for Year-2007 data. $\delta_{\text{sys}}(T_{AA} \oplus \text{pp norm.})$ are Type-C errors and show the absolute amount that the data points would move.

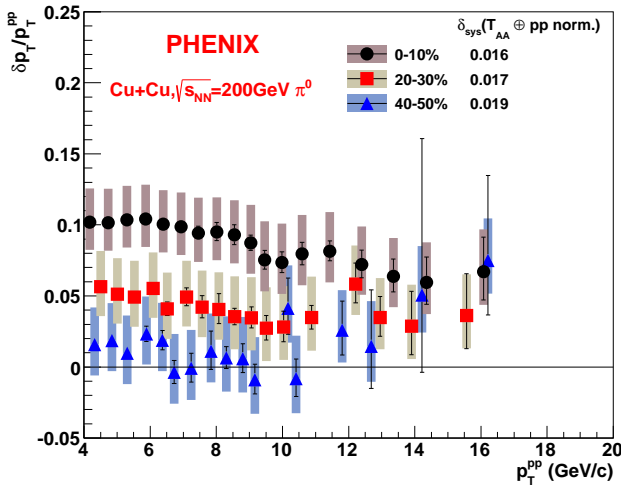


FIG. 4. (Color online) p_T^{pp} dependence of S_{loss} for π^0 in 200 GeV Cu+Cu collisions using the spectra measured by PHENIX at RHIC in 2005 [13]. $\delta_{\text{sys}}(T_{AA} \oplus \text{pp norm.})$ are Type-C errors and show the absolute amount that the data points would move.

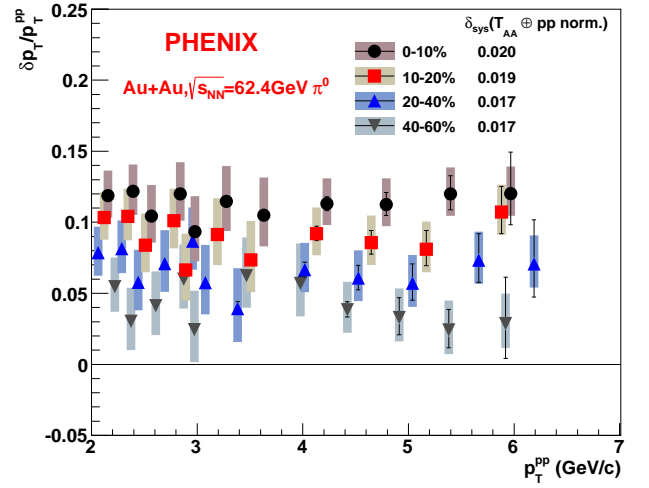


FIG. 5. (Color online) p_T^{pp} dependence of S_{loss} for π^0 in 62.4 GeV Au+Au collisions using the spectra measured by PHENIX in 2010 [7]. $\delta_{\text{sys}}(T_{AA} \oplus \text{pp norm.})$ are Type-C errors and show the absolute amount that the data points would move.

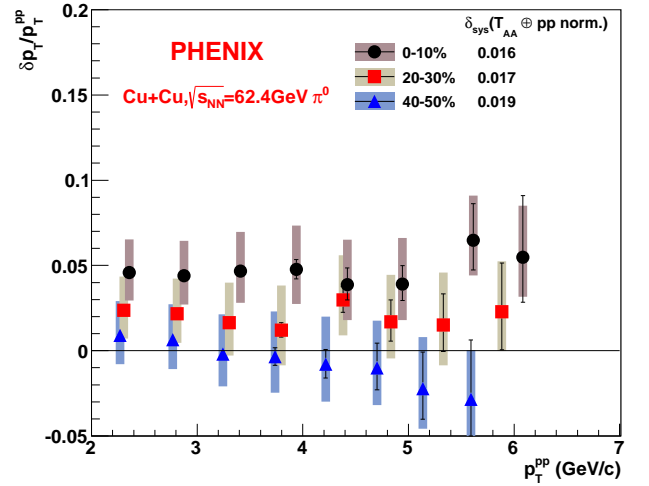


FIG. 6. (Color online) p_T^{pp} dependence of S_{loss} for π^0 in 62.4 GeV Cu+Cu collisions using the spectra measured by PHENIX in 2005 [13]. $\delta_{\text{sys}}(T_{AA} \oplus \text{pp norm.})$ are Type-C errors and show the absolute amount that the data points would move.

tively. Note that at these p_T^{pp} values, only data from 200 GeV and 2.76 TeV are available. When a value at the exact p_T^{pp} was not available, we interpolated the fractional momentum loss from the closest two p_T points that we obtained in the previous section. The error bars represent Type A and the boxes are Type B uncertainties; Type C uncertainties are not shown here. The scaling variable dependencies show clearer power-law behavior at $p_T = 12$ GeV/c than at $p_T = 7$ GeV/c, implying that

the S_{loss} is dominated by a single source, i.e., hard scattering. At fixed $\sqrt{s_{NN}}$, the S_{loss} values for the Cu+Cu and Au+Au systems converge as N_{part} grows. For the different $\sqrt{s_{NN}}$ values, a clear separation of S_{loss} values is seen even at the highest N_{part} , and the separation increases with increasing p_T (see Fig. 12).

Figures 12–15 show the same S_{loss} dependencies for additional p_T^{pp} values of 5–15 GeV/c. For the lowest two p_T^{pp} values, the results now also include Cu+Cu and Au+Au at $\sqrt{s_{NN}} = 62.4$ GeV. Note that the PHENIX and ALICE data show parallel trends as a function of N_{part} , especially at higher N_{part} . This fact, albeit the magnitudes

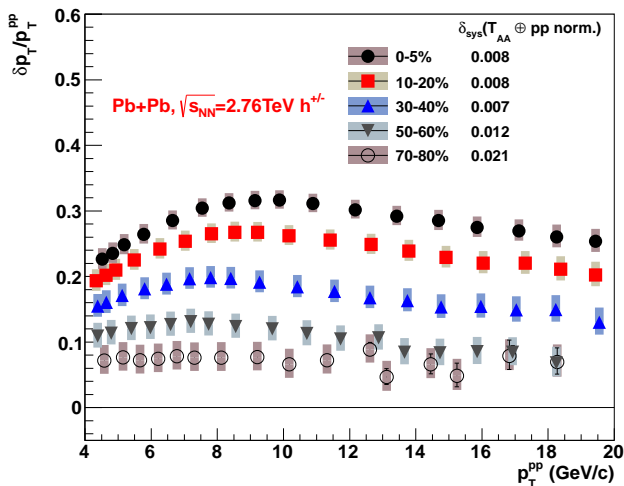


FIG. 7. (Color online) p_T^{pp} dependence of S_{loss} for charged hadrons in 2.76 TeV Pb+Pb collisions using the result from the ALICE experiment [16, 19]. $\delta_{\text{sys}}(T_{AA} \oplus \text{pp norm.})$ are Type-C errors and show the absolute amount that the data points would move.

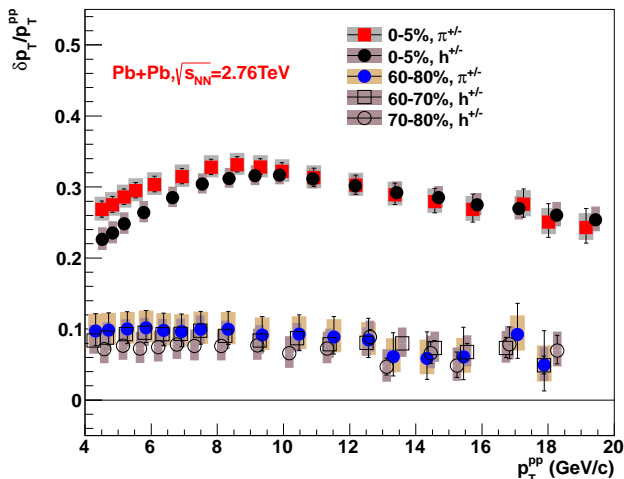


FIG. 8. (Color online) p_T^{pp} dependence of S_{loss} for charged pions in 2.76 TeV Pb+Pb collisions together with those for charged hadrons from the same collision system. The charged pion result is from the ALICE experiment [17].

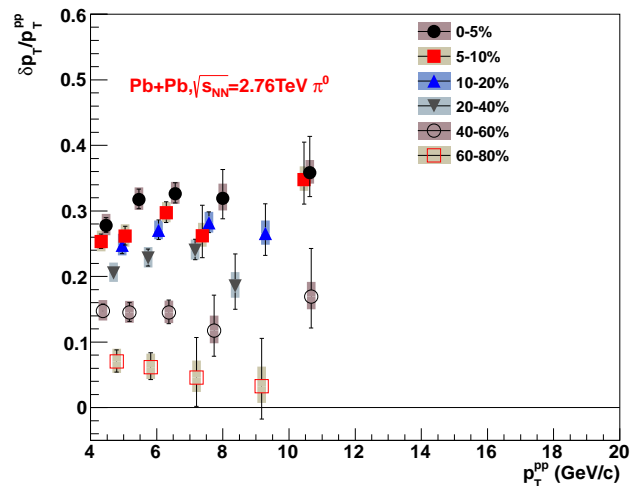


FIG. 9. (Color online) p_T^{pp} dependence of S_{loss} for neutral pions in 2.76 TeV Pb+Pb collisions using the result from the ALICE experiment [18].

At higher centralities (increasing $dN_{\text{ch}}/d\eta$) the LHC points line up very well with the 200 GeV RHIC Au+Au data, moreover, at higher p_T the two results are consistent for all but the most peripheral collisions. This clearly shows that S_{loss} scales with $dN_{\text{ch}}/d\eta$, which is energy density dependent and thus $\sqrt{s_{NN}}$ dependent. Finally, plots of S_{loss} as a function of $\varepsilon_{\text{Bj}}\tau_0$ 15 show remarkable universal trends for the data from different systems from 200 GeV to 2.76 TeV. Among the scaling variables, $dN_{\text{ch}}/d\eta$ and $\varepsilon_{\text{Bj}}\tau_0$ seems to serve best across the collision systems, especially between 200 GeV Au+Au and 2.76 TeV collisions. This investigation shows that the S_{loss} does not scale with simple geometry descriptions across the $\sqrt{s_{NN}}$, but do scale with the quantities related to the energy density of the system, hence the opacity of the system is energy-density dependent.

We have investigated S_{loss} against the four scaling variables at six p_T^{pp} points including the two already shown in Figs. 10 and 11. The scaling plots at all p_T^{pp} are shown in Figs. 12 – 15. For p_T of 5 and 6 GeV/c, we used the 2004 data, because the 2007 data has a software threshold in p_T , as mentioned earlier. At the same two lowest p_T , we also show the S_{loss} scaling for 62.4 GeV Cu+Cu and Au+Au collisions. For higher p_T the 62.4 GeV points are not available owing to the lack of a $p+p$ baseline. Deviations seen in the 62.4 GeV data may indicate that in the measured p_T range hard scattering is not completely dominant yet, in accordance with the observations of [7]. Lastly, to quantify the scaling trends, we fit S_{loss} for all four scaling variables and each collision system, except for $\sqrt{s_{NN}} = 62.4$ GeV system, with a power-law function:

$$\delta p_T / p_T = \beta (SV / SV^0)^\alpha \quad (7)$$

where SV is one of the four scaling variables we used above, and the SV^0 is the normalization factor introduced to cancel the dimension of the SV . We took the

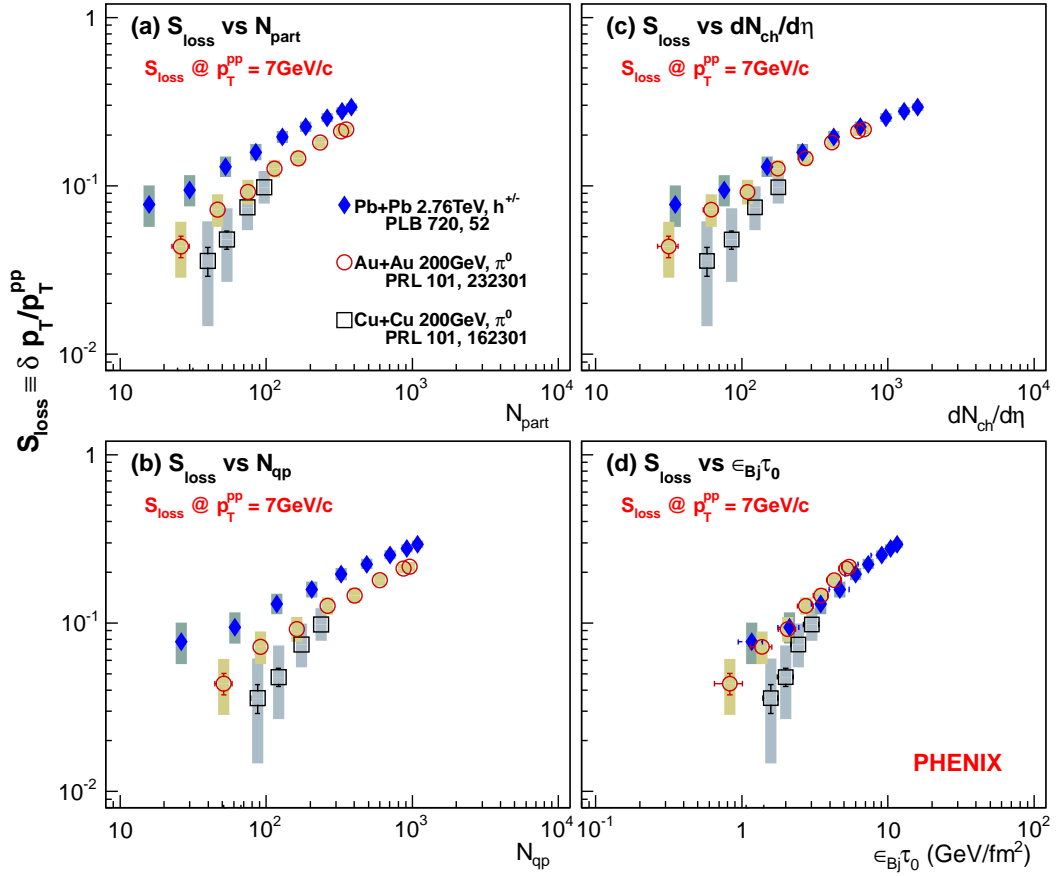


FIG. 10. (Color online) Scaling variables dependence of S_{loss} at $p_T^{\text{pp}} = 7$ GeV/c. (a) shows S_{loss} vs N_{part} , (b) shows S_{loss} vs N_{qp} , (c) shows S_{loss} vs $dN_{\text{ch}}/d\eta$, and (d) shows S_{loss} vs $\varepsilon_{\text{Bj}}\tau_0$. N_{qp} are all calculated by PHENIX. $\delta_{\text{sys}}(T_{\text{AA}} \oplus \text{pp norm})$ is not shown in these plots.

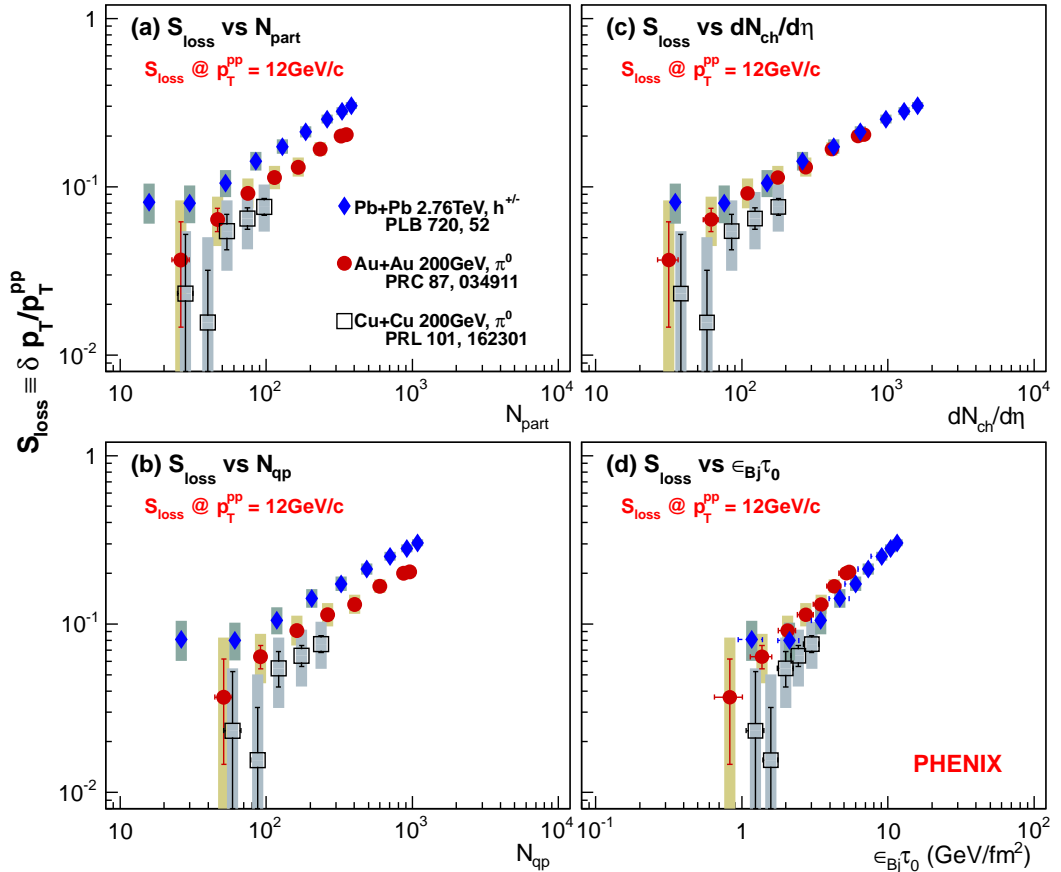


FIG. 11. (Color online) Scaling variables dependence of S_{loss} at $p_T^{\text{pp}} = 12$ GeV/c. (a) shows S_{loss} vs N_{part} , (b) shows S_{loss} vs N_{qp} , (c) shows S_{loss} vs $dN_{\text{ch}}/d\eta$, and (d) shows S_{loss} vs $\varepsilon_{\text{Bj}}\tau_0$. N_{qp} are all calculated by PHENIX. $\delta_{\text{sys}}(T_{\text{AA}} \oplus \text{pp norm})$ is not shown in these plots.

scaling variables for the most central LHC points as SV^0 .
 Use of the power-law function is motivated by an energy
 loss model that predicts that $\Delta E/E \propto N_{\text{part}}^{2/3}$ [31]. In
 the fitting process the statistical and systematic uncer-
 tainties were taken into account according to the pre-
 scription of [32]. The errors on the scaling variable (hor-
 izontal errors in the plots) are not taken into account in
 the fitting, but they are small compared to the uncer-
 tainties of S_{loss} values.

The fit parameters α and β obtained by fitting $\delta p_T/p_T$
 vs N_{part} and N_{qp} , plus $dN_{\text{ch}}/d\eta$ and $\varepsilon_{\text{Bj}}\tau_0$ to Eq. 7
 for Au+Au at $\sqrt{s_{NN}} = 200$ GeV and Pb+Pb at $\sqrt{s_{NN}}$
 $= 2.76$ TeV are shown in Fig. 16. All fit parameters,
 including for Cu+Cu, are tabulated in Table VII.

The fit parameters α and β are anti-correlated. At
 and above 10 GeV/c, the χ^2/ndf values ~~are small~~
become smaller and the powers α converge for all scal-
 ing variables, although they do not become fully consis-
 tent within uncertainties. Among the scaling variables,
 $dN_{\text{ch}}/d\eta$ is found to give relatively consistent α and β
 between two systems. The $\varepsilon_{\text{Bj}}\tau_0$, which is more related
 to the energy density of the system, also gives reasonably
 consistent numbers within uncertainties. More interest-
 ingly, $\varepsilon_{\text{Bj}}\tau_0$ gives the α closest to 1.0 (linear scaling). The
 similarities are striking as is the fact that S_{loss} obeys such
 a simple scaling with global observables over the entire
 p_T range where hard scattering is dominant. This im-
 plies that the empirical fractional momentum loss and
 the assumed underlying energy loss of partons scale with
 energy density of the medium, independent of the colli-
 sion energies or systems, once $\sqrt{s_{NN}}$ is sufficiently high.
 We cross-checked our current result with one published
 earlier for a slightly different quantity [12], and found
 consistent for $\sqrt{s_{NN}} = 200$ GeV Au+Au collisions.

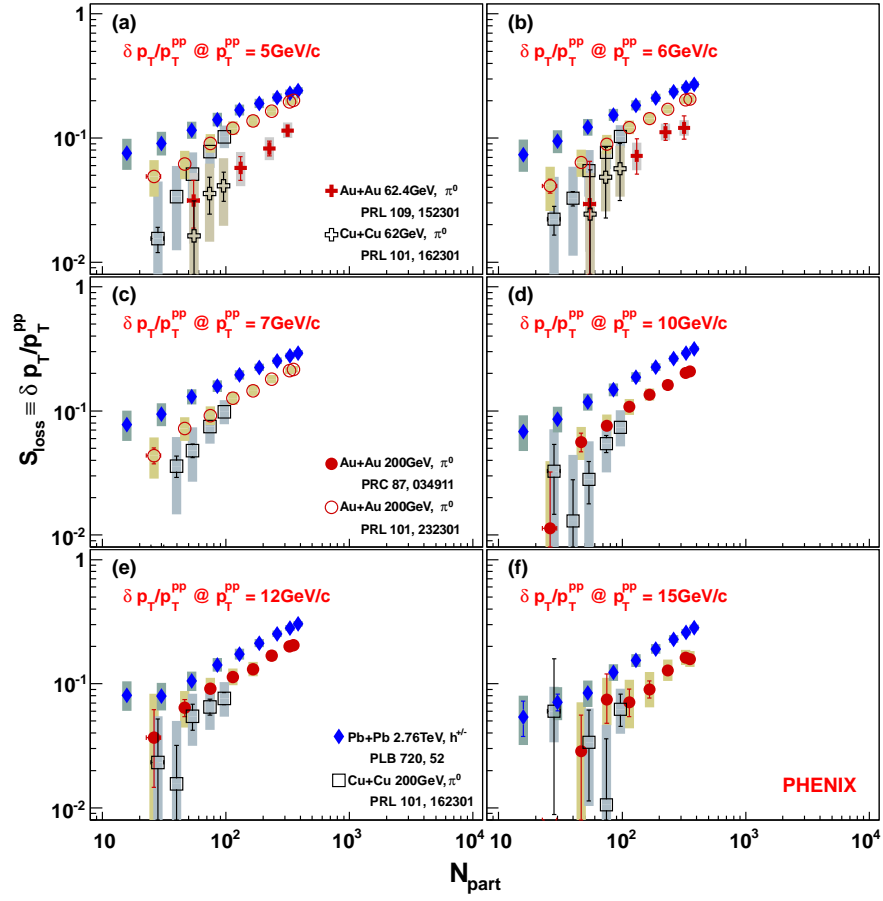


FIG. 12. (Color online) N_{part} dependence of the fractional momentum loss in bins of p_T^{pp} for various systems and $\sqrt{s_{NN}}$. $\delta_{\text{sys}}(T_{AA} \oplus \text{pp norm})$ is not shown in these plots.

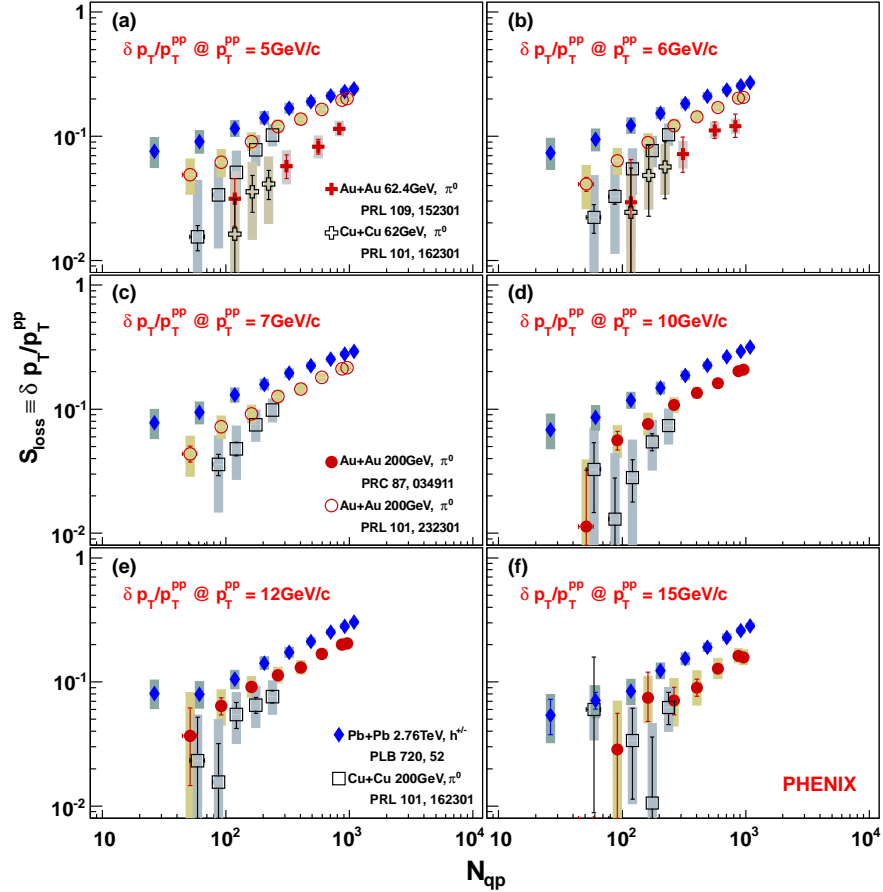


FIG. 13. (Color online) N_{qp} dependence of the fractional momentum loss in bins of p_T for various systems and $\sqrt{s_{NN}}$. $\delta_{\text{sys}}(T_{AA} \oplus \text{pp norm})$ is not shown in these plots. N_{qp} are all calculated by PHENIX.

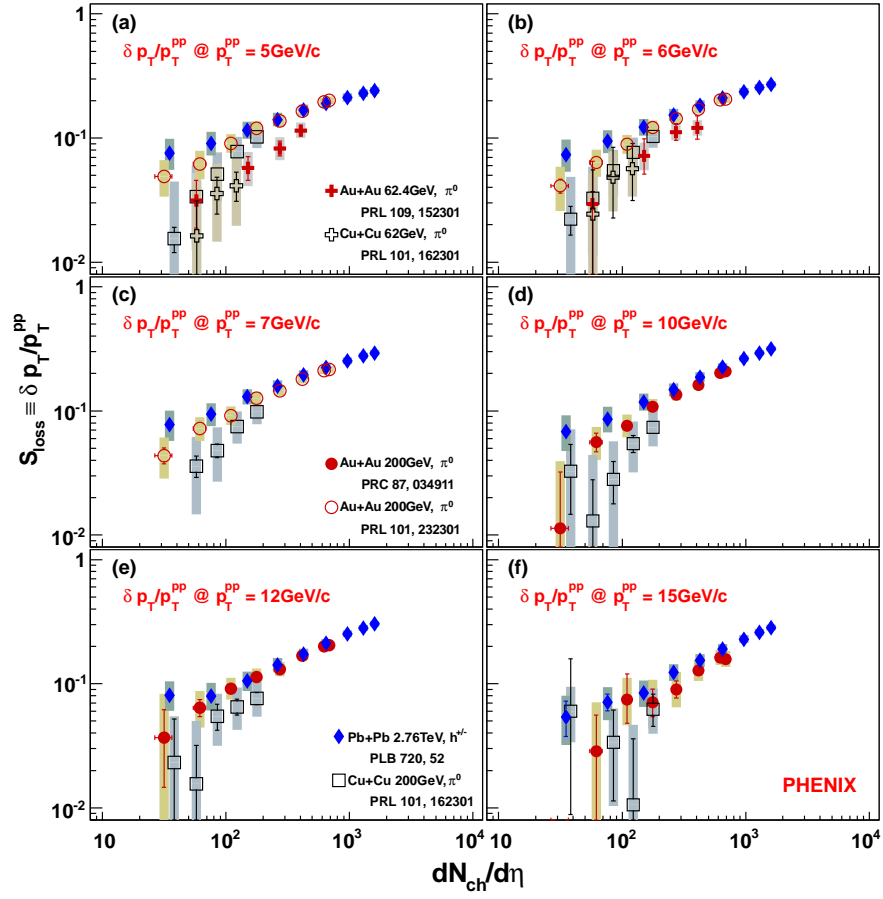


FIG. 14. (Color online) $dN_{ch}/d\eta$ dependence of the fractional momentum loss. $\delta_{sys}(T_{AA} \oplus pp \text{ norm})$ is not shown in these plots.

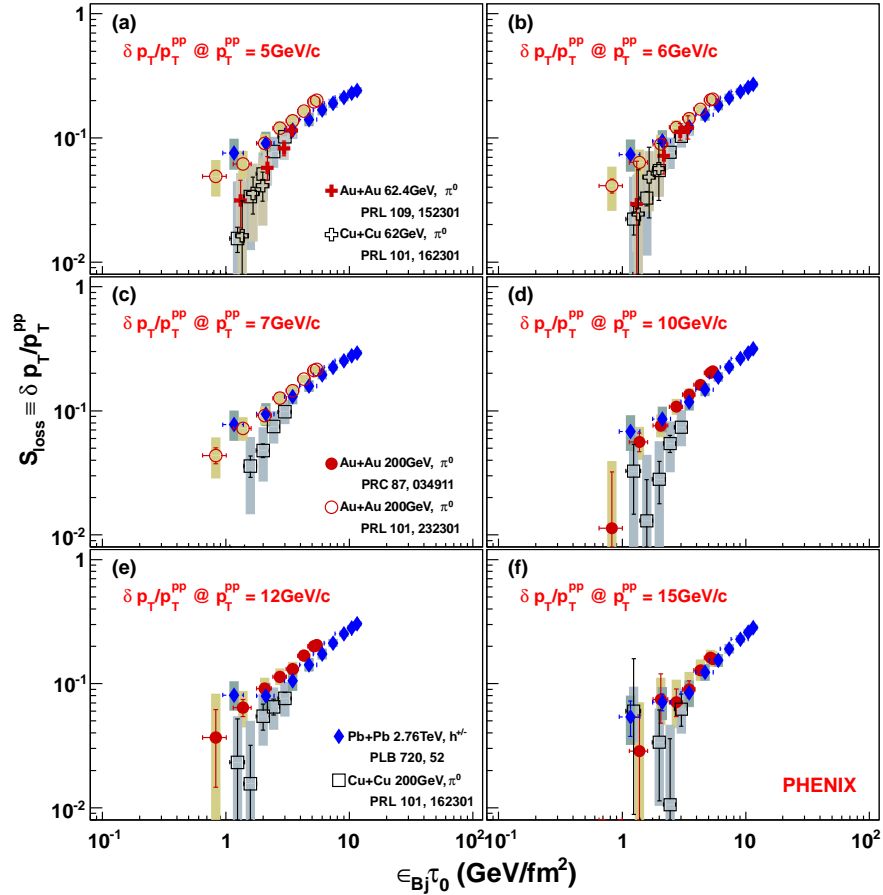


FIG. 15. (Color online) $\epsilon_{Bj}\tau_0$ dependence of the fractional momentum loss. $\delta_{sys}(T_{AA} \oplus pp \text{ norm})$ is not shown in these plots.

IV. SUMMARY

We have studied fractional momentum loss ($S_{\text{loss}} \equiv \delta p_T/p_T$) over various systems and collision energies as a function of p_T and four scaling variables: N_{part} , N_{qp} , $dN_{\text{ch}}/d\eta$ and $\varepsilon_{\text{Bj}}\tau_0$. We found that the same universal function of $dN_{\text{ch}}/d\eta$ or $\varepsilon_{\text{Bj}}\tau_0$ describes S_{loss} at RHIC ($\sqrt{s_{NN}} = 200$ GeV) and LHC ($\sqrt{s_{NN}} = 2.76$ TeV), while N_{part} and N_{qp} do not. This finding shows that the S_{loss} does not scale simply with system size across the $\sqrt{s_{NN}}$, but does scale with quantities related to the energy density of the system, implying that the opacity of the system is energy-density dependent. We quantitatively evaluated the slope of the universal curves for $\sqrt{s_{NN}} = 200$ and 2.76 TeV and again found that $dN_{\text{ch}}/d\eta$ and $\varepsilon_{\text{Bj}}\tau_0$ give relatively consistent α and β between two systems, and especially, that the α for $\varepsilon_{\text{Bj}}\tau_0$ is close to 1.0 (linear scaling). It is striking that S_{loss} obeys such a simple scaling with global observables over the entire p_T range where hard scattering is dominant. This implies that the empirical fractional momentum loss and the assumed underlying energy loss of partons scale with energy density of the medium, independent of the collision energies or systems, once $\sqrt{s_{NN}}$ is sufficiently high.

We propose that measurements of S_{loss} as well as the conventional R_{AA} , in the future, would provide important additional information to investigate the global feature of the energy loss of partons.

ACKNOWLEDGMENTS

We thank the staff of the Collider-Accelerator and Physics Departments at Brookhaven National Laboratory and the staff of the other PHENIX participating institutions for their vital contributions. We acknowledge support from the Office of Nuclear Physics in the Office of Science of the Department of Energy, the National Science Foundation, Abilene Christian University Research Council, Research Foundation of SUNY, and Dean of the College of Arts and Sciences, Vanderbilt University (U.S.A), Ministry of Education, Culture, Sports, Science, and Technology and the Japan Society for the Promotion of Science (Japan), Conselho Nacional de Desenvolvimento Científico e Tecnológico and Fundação de Amparo à Pesquisa do Estado de São Paulo (Brazil), Natural Science Foundation of China (P. R. China), Croatian Science Foundation and Ministry of Science, Education, and Sports (Croatia), Ministry of Education, Youth and Sports (Czech Republic), Centre National de la Recherche Scientifique, Commissariat à l'Énergie Atomique, and Institut National de Physique Nucléaire et de Physique des Particules (France), Bundesministerium für Bildung und Forschung, Deutscher Akademischer Austausch Dienst, and Alexander von Humboldt Stiftung (Germany), National Science Fund, OTKA, Károly Róbert University College, and the Ch. Simonyi Fund (Hungary), Department of Atomic Energy and De-

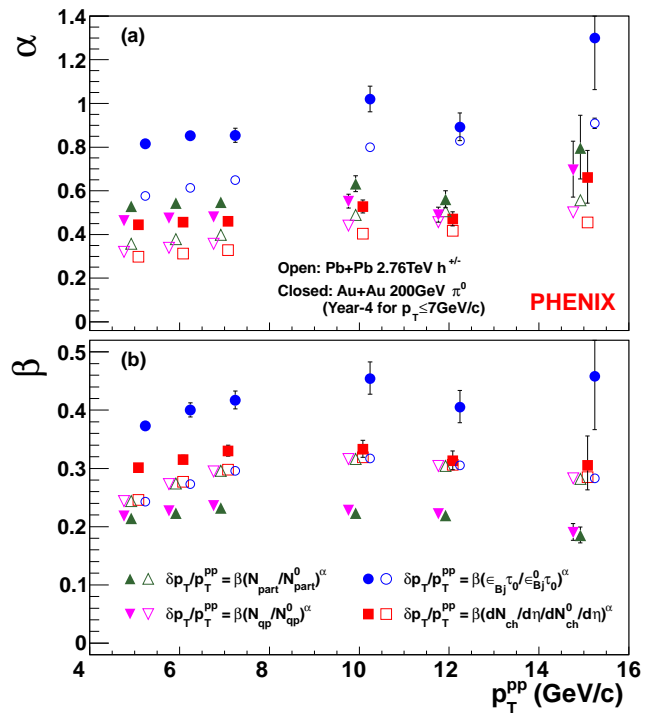


FIG. 16. (Color online) p_T^{pp} dependence of fitting parameters for S_{loss} vs scaling variables. Open symbols correspond to Pb+Pb 2.76 TeV, and closed symbols correspond to Au+Au 200 GeV. (a) α and (b) β vs p_T^{pp} . The Cu+Cu 200 GeV points are not shown, instead are tabulated in Table VII.

partment of Science and Technology (India), Israel Science Foundation (Israel), Basic Science Research Program through NRF of the Ministry of Education (Korea), Physics Department, Lahore University of Management Sciences (Pakistan), Ministry of Education and Science, Russian Academy of Sciences, Federal Agency of Atomic Energy (Russia), VR and Wallenberg Foundation (Sweden), the U.S. Civilian Research and Development Foundation for the Independent States of the Former Soviet Union, the Hungarian American Enterprise Scholarship Fund, and the US-Israel Binational Science Foundation.

APPENDIX

Tables of the centrality dependence of $\delta p_T/p_T^{\text{pp}}$ and parameters for fitting four different power-law functions for Au+Au and Cu+Cu data from the PHENIX experiment at RHIC and Pb+Pb data from the ALICE experiment at the LHC [16, 17, 30].

TABLE IV. Centrality dependence of $\delta p_T/p_T^{pp}$ in Au+Au collisions at $\sqrt{s_{NN}} = 200$ GeV from 2007 and 2004 data from the PHENIX experiment at RHIC.

Centrality	2007 data				2004 data			
	p_T^{pp} [GeV/c]	$\delta p_T/p_T^{pp}$	Stat error	Syst error	p_T^{pp} [GeV/c]	$\delta p_T/p_T^{pp}$	Stat error	Syst error
0%–5%	7.0	0.216	+0.004 –0.004	+0.015 –0.013	5.0	0.202	+0.003 –0.003	+0.015 –0.013
	10.0	0.209	+0.005 –0.005	+0.016 –0.014	6.0	0.206	+0.004 –0.003	+0.015 –0.013
	12.0	0.204	+0.007 –0.006	+0.016 –0.013	7.0	0.216	+0.002 –0.002	+0.015 –0.013
	15.0	0.157	+0.012 –0.010	+0.026 –0.021				
0%–10%	7.0	0.210	+0.001 –0.001	+0.016 –0.013	5.0	0.196	+0.002 –0.002	+0.015 –0.013
	10.0	0.202	+0.004 –0.004	+0.016 –0.014	6.0	0.202	+0.002 –0.002	+0.015 –0.013
	12.0	0.200	+0.006 –0.005	+0.016 –0.013	7.0	0.211	+0.003 –0.003	+0.015 –0.013
	15.0	0.162	+0.010 –0.009	+0.026 –0.020				
10%–20%	7.0	0.172	+0.001 –0.001	+0.016 –0.014	5.0	0.165	+0.002 –0.002	+0.016 –0.014
	10.0	0.162	+0.005 –0.005	+0.016 –0.014	6.0	0.171	+0.002 –0.002	+0.015 –0.013
	12.0	0.168	+0.007 –0.006	+0.017 –0.014	7.0	0.180	+0.003 –0.003	+0.015 –0.013
	15.0	0.128	+0.012 –0.011	+0.029 –0.022				
20%–30%	7.0	0.140	+0.002 –0.002	+0.017 –0.015	5.0	0.137	+0.002 –0.002	+0.016 –0.014
	10.0	0.135	+0.006 –0.005	+0.016 –0.014	6.0	0.144	+0.003 –0.002	+0.016 –0.014
	12.0	0.131	+0.006 –0.006	+0.019 –0.016	7.0	0.145	+0.003 –0.003	+0.016 –0.014
	15.0	0.090	+0.016 –0.014	+0.034 –0.026				
30%–40%	7.0	0.110	+0.002 –0.002	+0.018 –0.015	5.0	0.120	+0.002 –0.002	+0.016 –0.014
	10.0	0.108	+0.006 –0.006	+0.017 –0.015	6.0	0.122	+0.003 –0.003	+0.016 –0.014
	12.0	0.113	+0.007 –0.007	+0.019 –0.016	7.0	0.126	+0.004 –0.004	+0.016 –0.014
	15.0	0.071	+0.020 –0.016	+0.037 –0.027				
40%–50%	7.0	0.080	+0.002 –0.002	+0.018 –0.016	5.0	0.091	+0.002 –0.002	+0.017 –0.015
	10.0	0.076	+0.008 –0.007	+0.017 –0.015	6.0	0.089	+0.003 –0.003	+0.017 –0.015
	12.0	0.091	+0.008 –0.007	+0.020 –0.017	7.0	0.092	+0.004 –0.004	+0.017 –0.015
	15.0	0.075	+0.045 –0.027	+0.037 –0.028				
50%–60%	7.0	0.055	+0.003 –0.003	+0.019 –0.016	5.0	0.062	+0.003 –0.003	+0.017 –0.015
	10.0	0.056	+0.010 –0.009	+0.018 –0.016	6.0	0.064	+0.004 –0.004	+0.017 –0.015
	12.0	0.064	+0.011 –0.010	+0.023 –0.019	7.0	0.072	+0.005 –0.005	+0.017 –0.015
	15.0	0.029	+0.027 –0.022	+0.042 –0.031				
60%–70%	7.0	0.028	+0.004 –0.004	+0.019 –0.017	5.0	0.049	+0.003 –0.003	+0.017 –0.015
	10.0	0.011	+0.021 –0.019	+0.028 –0.024	6.0	0.041	+0.006 –0.005	+0.018 –0.015
	12.0	0.037	+0.025 –0.022	+0.046 –0.037	7.0	0.044	+0.007 –0.006	+0.018 –0.015
	15.0	-0.098	+0.046 –0.063	+0.053 –0.077				

TABLE V. Centrality dependence of $\delta p_T/p_T^{pp}$ in Au+Au collisions at $\sqrt{s_{NN}} = 62.4$ GeV and Cu+Cu collisions at $\sqrt{s_{NN}} = 200$ and 62.4 GeV from the PHENIX experiment at RHIC.

System	Centrality	p_T^{pp}	$\delta p_T/p_T^{pp}$	stat	syst	System	Centrality	p_T^{pp}	$\delta p_T/p_T^{pp}$	stat	syst
$\sqrt{s_{NN}}$		[GeV/c]		uncert.	uncert.	$\sqrt{s_{NN}}$		[GeV/c]		uncert.	uncert.
Au+Au 62.4 GeV	0%–10%	5.0	0.115	+0.010 –0.009	+0.018 –0.015	Cu+Cu 200 GeV (continued)	30%–40%	5.0	0.034	+0.002 –0.002	+0.026 –0.021
		6.0	0.120	+0.030 –0.023	+0.019 –0.016			6.0	0.033	+0.004 –0.004	+0.026 –0.021
	10%–20%	5.0	0.083	+0.012 –0.010	+0.019 –0.016			7.0	0.036	+0.007 –0.007	+0.026 –0.021
		6.0	0.112	+0.019 –0.016	+0.019 –0.016			10.0	0.013	+0.015 –0.013	+0.031 –0.025
								12.0	0.016	+0.016 –0.015	+0.035 –0.028
								15.0	-0.001	+0.028 –0.035	+0.028 –0.035
	20%–40%	5.0	0.057	+0.013 –0.012	+0.020 –0.016						
		6.0	0.072	+0.027 –0.021	+0.020 –0.017		40%–50%	5.0	0.015	+0.004 –0.004	+0.029 –0.024
								6.0	0.022	+0.006 –0.006	+0.027 –0.022
								7.0	-0.002	+0.015 –0.016	+0.034 –0.042
								10.0	0.033	+0.021 –0.018	+0.038 –0.031
								12.0	0.023	+0.029 –0.023	+0.031 –0.025
								15.0	0.060	+0.099 –0.051	+0.034 –0.026
Cu+Cu 200 GeV	0%–10%	5.0	0.102	+0.001 –0.001	+0.024 –0.020	Cu+Cu 62.4 GeV	0%–10%	5.0	0.041	+0.012 –0.010	+0.028 –0.022
		6.0	0.103	+0.002 –0.002	+0.024 –0.020			6.0	0.057	+0.034 –0.025	+0.030 –0.023
		7.0	0.098	+0.004 –0.004	+0.024 –0.020						
		10.0	0.074	+0.008 –0.007	+0.027 –0.022						
		12.0	0.076	+0.009 –0.008	+0.027 –0.022						
		15.0	0.062	+0.020 –0.017	+0.029 –0.023						
	10%–20%	5.0	0.078	+0.002 –0.002	+0.024 –0.020		10%–20%	5.0	0.036	+0.013 –0.011	+0.027 –0.021
		6.0	0.077	+0.003 –0.003	+0.024 –0.020			6.0	0.048	+0.035 –0.026	+0.030 –0.023
		7.0	0.075	+0.005 –0.004	+0.025 –0.020						
		10.0	0.054	+0.009 –0.008	+0.028 –0.022						
		12.0	0.065	+0.010 –0.009	+0.028 –0.022						
		15.0	0.011	+0.025 –0.021	+0.036 –0.027						
	20%–30%	5.0	0.051	+0.002 –0.002	+0.025 –0.021		20%–30%	5.0	0.016	+0.015 –0.013	+0.029 –0.022
		6.0	0.054	+0.004 –0.004	+0.025 –0.021			6.0	0.024	+0.031 –0.024	+0.028 –0.022
		7.0	0.048	+0.006 –0.006	+0.026 –0.021						
		10.0	0.028	+0.011 –0.010	+0.029 –0.023						
		12.0	0.055	+0.014 –0.012	+0.029 –0.023		30%–40%	5.0	0.005	+0.028 –0.024	+0.056 –0.044
								6.0	-0.010	+0.127 –0.163	+0.137 –0.180
		15.0	0.034	+0.028 –0.022	+0.029 –0.023						
	40%–50%	5.0					40%–50%	5.0	-0.019	+0.018 –0.021	+0.026 –0.033
		6.0						6.0	-0.034	+0.035 –0.050	+0.019 –0.024

TABLE VI. Centrality dependence of $\delta p_T/p_T^{pp}$ Pb+Pb collisions at $\sqrt{s_{NN}} = 2.76$ TeV from the spectra measured by the ALICE experiment at the LHC [16, 17, 30].

Centrality	p_T^{pp} [GeV/c]	$\delta p_T/p_T^{pp}$	Stat error	Syst error	Centrality	p_T^{pp} [GeV/c]	$\delta p_T/p_T^{pp}$	Stat error	Syst error
0%–5%	5.0	0.241	+0.001 –0.001	+0.017 –0.015	30%–40%	10.0	0.187	+0.002 –0.002	+0.018 –0.016
	6.0	0.270	+0.001 –0.001	+0.016 –0.014	(continued)	12.0	0.173	+0.002 –0.002	+0.018 –0.016
	7.0	0.293	+0.001 –0.001	+0.015 –0.014		15.0	0.154	+0.004 –0.004	+0.020 –0.017
	10.0	0.316	+0.001 –0.001	+0.015 –0.013					
	12.0	0.303	+0.001 –0.001	+0.015 –0.013	40%–50%	5.0	0.141	+0.001 –0.001	+0.019 –0.017
	15.0	0.282	+0.002 –0.002	+0.016 –0.014		6.0	0.153	+0.001 –0.001	+0.019 –0.016
5%–10%	5.0	0.229	+0.001 –0.001	+0.017 –0.015		7.0	0.158	+0.001 –0.001	+0.019 –0.016
	6.0	0.255	+0.001 –0.001	+0.016 –0.014		10.0	0.148	+0.002 –0.002	+0.019 –0.017
	7.0	0.277	+0.001 –0.001	+0.016 –0.014		12.0	0.142	+0.003 –0.003	+0.019 –0.017
	10.0	0.293	+0.001 –0.001	+0.015 –0.014		15.0	0.123	+0.005 –0.005	+0.021 –0.018
	12.0	0.281	+0.002 –0.002	+0.016 –0.014	50%–60%	5.0	0.116	+0.001 –0.001	+0.020 –0.017
	15.0	0.259	+0.003 –0.002	+0.017 –0.015		6.0	0.122	+0.001 –0.001	+0.020 –0.017
10%–20%	5.0	0.211	+0.001 –0.001	+0.017 –0.015		7.0	0.130	+0.002 –0.002	+0.020 –0.017
	6.0	0.236	+0.001 –0.001	+0.017 –0.015		10.0	0.118	+0.003 –0.003	+0.020 –0.018
	7.0	0.253	+0.001 –0.001	+0.016 –0.014		12.0	0.105	+0.004 –0.004	+0.021 –0.018
	10.0	0.263	+0.001 –0.001	+0.016 –0.014		15.0	0.084	+0.007 –0.007	+0.022 –0.019
	12.0	0.252	+0.002 –0.001	+0.016 –0.014	60%–70%	5.0	0.091	+0.002 –0.002	+0.021 –0.019
	15.0	0.228	+0.002 –0.002	+0.018 –0.015		6.0	0.094	+0.002 –0.002	+0.021 –0.019
20%–30%	5.0	0.190	+0.001 –0.001	+0.018 –0.015		7.0	0.094	+0.003 –0.002	+0.021 –0.019
	6.0	0.210	+0.001 –0.001	+0.017 –0.015		10.0	0.086	+0.004 –0.004	+0.022 –0.019
	7.0	0.224	+0.001 –0.001	+0.017 –0.015		12.0	0.080	+0.006 –0.006	+0.022 –0.019
	10.0	0.224	+0.001 –0.001	+0.017 –0.015		15.0	0.071	+0.011 –0.010	+0.023 –0.020
	12.0	0.212	+0.002 –0.002	+0.017 –0.015	70%–80%	5.0	0.075	+0.003 –0.003	+0.023 –0.020
	15.0	0.190	+0.003 –0.003	+0.019 –0.016		6.0	0.074	+0.003 –0.003	+0.024 –0.020
30%–40%	5.0	0.168	+0.001 –0.001	+0.018 –0.016		7.0	0.077	+0.004 –0.004	+0.023 –0.020
	6.0	0.183	+0.001 –0.001	+0.018 –0.016		10.0	0.068	+0.006 –0.006	+0.024 –0.021
	7.0	0.195	+0.001 –0.001	+0.018 –0.015		12.0	0.081	+0.010 –0.009	+0.024 –0.020
						15.0	0.054	+0.019 –0.017	+0.026 –0.022

TABLE VII. Parameters from fitting the indicated power-law functions for $\delta p_T/p_T$ to the data as a function of p_T^{pp} for Au+Au collisions from 2004 and 2007 data and for Cu+Cu collisions from 2005 data at $\sqrt{s_{NN}} = 200$ GeV.

System	$\sqrt{s_{NN}}$	year	hadron	$\delta p_T/p_T =$	p_T^{pp}	α	β	χ^2/ndf
Au+Au	200 GeV	2004	π^0	$\beta(N_{\text{part}}/N_{\text{part}}^0)^\alpha$	5 GeV/c	$0.529^{+0.011}_{-0.011}$	$2.14^{+0.04}_{-0.03} \times 10^{-1}$	25.45/5
					6 GeV/c	$0.543^{+0.015}_{-0.015}$	$2.23^{+0.04}_{-0.04} \times 10^{-1}$	15.56/5
					7 GeV/c	$0.548^{+0.020}_{-0.020}$	$2.32^{+0.05}_{-0.04} \times 10^{-1}$	7.11/5
				$\beta(N_{\text{qp}}/N_{\text{qp}}^0)^\alpha$	5 GeV/c	$0.463^{+0.010}_{-0.010}$	$2.18^{+0.04}_{-0.04} \times 10^{-1}$	23.35/5
					6 GeV/c	$0.475^{+0.013}_{-0.013}$	$2.27^{+0.04}_{-0.04} \times 10^{-1}$	15.23/5
					7 GeV/c	$0.480^{+0.017}_{-0.017}$	$2.36^{+0.05}_{-0.05} \times 10^{-1}$	7.50/5
				$\beta(dN_{ch}/d\eta/dN_{ch}^0/d\eta)^\alpha$	5 GeV/c	$0.445^{+0.009}_{-0.009}$	$3.01^{+0.06}_{-0.06} \times 10^{-1}$	27.78/5
					6 GeV/c	$0.456^{+0.013}_{-0.013}$	$3.15^{+0.08}_{-0.07} \times 10^{-1}$	18.56/5
					7 GeV/c	$0.460^{+0.017}_{-0.016}$	$3.30^{+0.10}_{-0.09} \times 10^{-1}$	8.50/5
				$\beta(\epsilon\tau_0/\epsilon^0\tau_0)^\alpha$	5 GeV/c	$0.815^{+0.018}_{-0.018}$	$3.73^{+0.09}_{-0.09} \times 10^{-1}$	14.67/5
					6 GeV/c	$0.852^{+0.025}_{-0.025}$	$4.00^{+0.12}_{-0.12} \times 10^{-1}$	3.79/5
					7 GeV/c	$0.854^{+0.032}_{-0.032}$	$4.17^{+0.16}_{-0.15} \times 10^{-1}$	4.23/5
			π^0	$\beta(N_{\text{part}}/N_{\text{part}}^0)^\alpha$	10 GeV/c	$0.632^{+0.036}_{-0.035}$	$2.23^{+0.06}_{-0.06} \times 10^{-1}$	3.31/5
					12 GeV/c	$0.561^{+0.040}_{-0.038}$	$2.19^{+0.07}_{-0.07} \times 10^{-1}$	1.75/5
					15 GeV/c	$0.795^{+0.151}_{-0.141}$	$1.85^{+0.14}_{-0.13} \times 10^{-1}$	4.68/5
				$\beta(N_{\text{qp}}/N_{\text{qp}}^0)^\alpha$	10 GeV/c	$0.552^{+0.032}_{-0.031}$	$2.28^{+0.06}_{-0.06} \times 10^{-1}$	3.32/5
					12 GeV/c	$0.490^{+0.035}_{-0.034}$	$2.22^{+0.07}_{-0.07} \times 10^{-1}$	1.78/5
					15 GeV/c	$0.695^{+0.132}_{-0.124}$	$1.90^{+0.15}_{-0.14} \times 10^{-1}$	4.74/5
				$\beta(dN_{ch}/d\eta/dN_{ch}^0/d\eta)^\alpha$	10 GeV/c	$0.528^{+0.030}_{-0.029}$	$3.33^{+0.15}_{-0.14} \times 10^{-1}$	3.72/5
					12 GeV/c	$0.471^{+0.033}_{-0.032}$	$3.13^{+0.17}_{-0.15} \times 10^{-1}$	1.59/5
					15 GeV/c	$0.661^{+0.124}_{-0.117}$	$3.05^{+0.51}_{-0.42} \times 10^{-1}$	4.69/5
				$\beta(\epsilon\tau_0/\epsilon^0\tau_0)^\alpha$	10 GeV/c	$1.020^{+0.060}_{-0.058}$	$4.54^{+0.29}_{-0.26} \times 10^{-1}$	2.05/5
					12 GeV/c	$0.892^{+0.064}_{-0.063}$	$4.05^{+0.29}_{-0.27} \times 10^{-1}$	2.43/5
					15 GeV/c	$1.300^{+0.255}_{-0.237}$	$4.58^{+1.23}_{-0.91} \times 10^{-1}$	4.36/5
Cu+Cu	200 GeV	2005	π^0	$\beta(N_{\text{part}}/N_{\text{part}}^0)^\alpha$	5 GeV/c	$1.210^{+0.046}_{-0.045}$	$5.45^{+0.41}_{-0.37} \times 10^{-1}$	8.28/3
					6 GeV/c	$1.180^{+0.082}_{-0.079}$	$5.21^{+0.70}_{-0.60} \times 10^{-1}$	1.48/3
					7 GeV/c	$1.200^{+0.148}_{-0.141}$	$5.17^{+1.31}_{-1.01} \times 10^{-1}$	2.92/3
				$\beta(N_{\text{qp}}/N_{\text{qp}}^0)^\alpha$	5 GeV/c	$1.060^{+0.040}_{-0.039}$	$5.21^{+0.38}_{-0.35} \times 10^{-1}$	9.71/3
					6 GeV/c	$1.030^{+0.072}_{-0.069}$	$4.99^{+0.65}_{-0.56} \times 10^{-1}$	1.69/3
					7 GeV/c	$1.060^{+0.130}_{-0.124}$	$4.94^{+1.21}_{-0.94} \times 10^{-1}$	3.07/3
				$\beta(dN_{ch}/d\eta/dN_{ch}^0/d\eta)^\alpha$	5 GeV/c	$0.940^{+0.035}_{-0.035}$	$8.22^{+0.74}_{-0.67} \times 10^{-1}$	15.46/3
					6 GeV/c	$0.917^{+0.063}_{-0.061}$	$7.80^{+1.26}_{-1.06} \times 10^{-1}$	2.26/3
					7 GeV/c	$0.931^{+0.113}_{-0.108}$	$7.70^{+2.39}_{-1.77} \times 10^{-1}$	3.81/3
				$\beta(\epsilon\tau_0/\epsilon^0\tau_0)^\alpha$	5 GeV/c	$1.670^{+0.063}_{-0.061}$	$9.83^{+0.96}_{-0.86} \times 10^{-1}$	15.29/3
					6 GeV/c	$1.630^{+0.112}_{-0.108}$	$9.28^{+1.64}_{-1.35} \times 10^{-1}$	1.92/3
					7 GeV/c	$1.650^{+0.202}_{-0.192}$	$9.18^{+3.12}_{-2.25} \times 10^{-1}$	3.88/3

TABLE VIII. Parameters from fitting the indicated power-law functions for $\delta p_T/p_T$ to the data as a function of p_T^{pp} for Pb+Pb collisions at $\sqrt{s_{NN}} = 2.76$ TeV.

System	$\sqrt{s_{NN}}$	year	hadron	$\delta p_T/p_T =$	p_T^{pp}	α	β	χ^2/ndf
Pb+Pb	2.76 TeV	2010-11	$h^{+/-}$	$\beta(N_{\text{part}}/N_{\text{part}}^0)^\alpha$	5 GeV/c	$0.357^{+0.004}_{-0.004}$	$2.44^{+0.04}_{-0.04} \times 10^{-1}$	44.19/7
					6 GeV/c	$0.378^{+0.004}_{-0.003}$	$2.74^{+0.04}_{-0.04} \times 10^{-1}$	90.44/7
					7 GeV/c	$0.398^{+0.004}_{-0.004}$	$2.96^{+0.05}_{-0.04} \times 10^{-1}$	70.86/7
					10 GeV/c	$0.490^{+0.006}_{-0.006}$	$3.16^{+0.05}_{-0.04} \times 10^{-1}$	10.32/7
					12 GeV/c	$0.507^{+0.008}_{-0.008}$	$3.04^{+0.05}_{-0.04} \times 10^{-1}$	11.41/7
				$\beta(N_{\text{qp}}/N_{\text{qp}}^0)^\alpha$	15 GeV/c	$0.557^{+0.014}_{-0.014}$	$2.82^{+0.05}_{-0.04} \times 10^{-1}$	2.29/7
					5 GeV/c	$0.320^{+0.003}_{-0.003}$	$2.44^{+0.04}_{-0.04} \times 10^{-1}$	34.51/7
					6 GeV/c	$0.339^{+0.003}_{-0.003}$	$2.73^{+0.04}_{-0.04} \times 10^{-1}$	71.06/7
					7 GeV/c	$0.358^{+0.003}_{-0.003}$	$2.95^{+0.05}_{-0.04} \times 10^{-1}$	59.14/7
					10 GeV/c	$0.440^{+0.005}_{-0.005}$	$3.16^{+0.05}_{-0.04} \times 10^{-1}$	9.62/7
				$\beta(dN_{ch}/d\eta/dN_{ch}^0/d\eta)^\alpha$	12 GeV/c	$0.456^{+0.007}_{-0.007}$	$3.04^{+0.05}_{-0.04} \times 10^{-1}$	13.94/7
					15 GeV/c	$0.501^{+0.013}_{-0.013}$	$2.83^{+0.05}_{-0.04} \times 10^{-1}$	2.30/7
					5 GeV/c	$0.298^{+0.003}_{-0.003}$	$2.46^{+0.04}_{-0.04} \times 10^{-1}$	66.71/7
					6 GeV/c	$0.313^{+0.003}_{-0.003}$	$2.77^{+0.04}_{-0.04} \times 10^{-1}$	145.00/7
					7 GeV/c	$0.329^{+0.003}_{-0.003}$	$2.98^{+0.05}_{-0.05} \times 10^{-1}$	123.28/7
				$\beta(\epsilon\tau_0/\epsilon^0\tau_0)^\alpha$	10 GeV/c	$0.404^{+0.005}_{-0.005}$	$3.19^{+0.05}_{-0.04} \times 10^{-1}$	30.94/7
					12 GeV/c	$0.417^{+0.006}_{-0.006}$	$3.06^{+0.05}_{-0.04} \times 10^{-1}$	26.21/7
					15 GeV/c	$0.455^{+0.011}_{-0.011}$	$2.85^{+0.05}_{-0.04} \times 10^{-1}$	5.76/7
					5 GeV/c	$0.576^{+0.006}_{-0.006}$	$2.43^{+0.04}_{-0.04} \times 10^{-1}$	53.83/7
					6 GeV/c	$0.614^{+0.006}_{-0.006}$	$2.73^{+0.04}_{-0.04} \times 10^{-1}$	91.36/7
					7 GeV/c	$0.649^{+0.006}_{-0.006}$	$2.96^{+0.05}_{-0.04} \times 10^{-1}$	79.47/7
					10 GeV/c	$0.799^{+0.009}_{-0.009}$	$3.17^{+0.05}_{-0.04} \times 10^{-1}$	32.58/7
					12 GeV/c	$0.829^{+0.013}_{-0.013}$	$3.05^{+0.05}_{-0.04} \times 10^{-1}$	30.78/7
					15 GeV/c	$0.909^{+0.023}_{-0.023}$	$2.83^{+0.05}_{-0.04} \times 10^{-1}$	6.28/7

-
- [1] K. Adcox *et al.* (PHENIX Collaboration), “Formation of dense partonic matter in relativistic nucleus-nucleus collisions at RHIC: Experimental evaluation by the PHENIX Collaboration,” Nucl. Phys. A **757**, 184 (2005).
- [2] I. Arsene *et al.* (BRAHMS), “Quark gluon plasma and color glass condensate at RHIC? The Perspective from the BRAHMS experiment,” Nucl. Phys. A **757**, 1–27 (2005), arXiv:nucl-ex/0410020 [nucl-ex].
- [3] B. B. Back *et al.*, “The PHOBOS perspective on discoveries at RHIC,” Nucl. Phys. A **757**, 28–101 (2005), arXiv:nucl-ex/0410022 [nucl-ex].
- [4] John Adams *et al.* (STAR), “Experimental and theoretical challenges in the search for the quark gluon plasma: The STAR Collaboration’s critical assessment of the evidence from RHIC collisions,” Nucl. Phys. A **757**, 102–183 (2005), arXiv:nucl-ex/0501009 [nucl-ex].
- [5] J. D. Bjorken, “Energy Loss of Energetic Partons in Quark - Gluon Plasma: Possible Extinction of High $p(t)$ Jets in Hadron-Hadron Collisions,” Report FERMILAB-PUB-82-059-THY (1982).
- [6] X.-N. Wang, “Effect of jet quenching on high p_T hadron spectra in high-energy nuclear collisions,” Phys. Rev. C **58**, 2321 (1998).
- [7] A. Adare *et al.* (PHENIX Collaboration), “Evolution of π^0 suppression in Au+Au collisions from $\sqrt{s_{NN}} = 39$ to 200 GeV,” Phys. Rev. Lett. **109**, 152301 (2012).
- [8] A. Adare *et al.* (PHENIX Collaboration), “Neutral pion production with respect to centrality and reaction plane in Au+Au collisions at $\sqrt{s_{NN}}=200$ GeV,” Phys. Rev. C **87**, 034911 (2013).
- [9] W. A. Horowitz and M. Gyulassy, “The Surprising Transparency of the sQGP at LHC,” Nucl. Phys. A **872**, 265 (2011).
- [10] S. S. Adler *et al.* (PHENIX Collaboration), “A Detailed Study of High- p_T Neutral-Pion Suppression and Azimuthal Anisotropy in Au+Au Collisions at $\sqrt{s_{NN}} = 200$ GeV,” Phys. Rev. C **76**, 034904 (2007).
- [11] P. Christiansen, K. Tywoniuk, and V. Vislavicius, “Universal scaling dependence of QCD energy loss from data driven studies,” Phys. Rev. C **89**, 034912 (2014).
- [12] A. Adare *et al.* (PHENIX Collaboration), “Suppression pattern of neutral pions at high transverse momentum in Au + Au collisions at $\sqrt{s_{NN}}=200$ GeV and constraints on medium transport coefficients,” Phys. Rev. Lett. **101**, 232301 (2008).
- [13] A. Adare *et al.* (PHENIX Collaboration), “Onset of π^0 Suppression Studied in Cu+Cu Collisions at $\sqrt{s_{NN}}=22.4, 62.4$, and 200 GeV,” Phys. Rev. Lett. **101**, 162301 (2008).
- [14] A. Adare *et al.* (PHENIX Collaboration), “Inclusive cross-section and double helicity asymmetry for π^0 production in $p + p$ collisions at $\sqrt{s} = 200$ GeV: Implications for the polarized gluon distribution in the proton,” Phys. Rev. D **76**, 051106 (2007).
- [15] A. Adare *et al.* (PHENIX Collaboration), “Inclusive cross section and double helicity asymmetry for π^0 production in $p + p$ collisions at $\sqrt{s} = 62.4$ GeV,” Phys. Rev. D **79**, 012003 (2009).
- [16] B. Abelev *et al.* (ALICE Collaboration), “Centrality Dependence of Charged Particle Production at Large Transverse Momentum in Pb-Pb Collisions at $\sqrt{s_{NN}} = 2.76$ TeV,” Phys. Lett. B **720**, 52 (2013).
- [17] B. B. Abelev *et al.* (ALICE Collaboration), “Production of charged pions, kaons and protons at large transverse momenta in pp and PbPb collisions at $\sqrt{s_{NN}}=2.76$ TeV,” Phys. Lett. B **736**, 196 (2014).
- [18] B. B. Abelev *et al.* (ALICE Collaboration), “Neutral pion production at midrapidity in pp and Pb-Pb collisions at $\sqrt{s_{NN}} = 2.76$ TeV,” Eur. Phys. J. **74**, 3108 (2014), and private communication with D. Peressounko and K. Reygers.
- [19] B. B. Abelev *et al.* (ALICE Collaboration), “Energy Dependence of the Transverse Momentum Distributions of Charged Particles in pp Collisions Measured by ALICE Collaboration,” Eur. Phys. J. **73**, 2662 (2013).
- [20] S. S. Adler *et al.* (PHENIX Collaboration), “Transverse-energy distributions at midrapidity in $p+p$, $d+Au$, and $Au+Au$ collisions at $\sqrt{s_{NN}} = 62.4$ –200 GeV and implications for particle-production models,” Phys. Rev. C **89**, 044905 (2014).
- [21] K. Aamodt *et al.* (ALICE Collaboration), “Centrality dependence of the charged-particle multiplicity density at mid-rapidity in Pb-Pb collisions at $\sqrt{s_{NN}}=2.76$ TeV,” Phys. Rev. Lett. **106**, 032301 (2011).
- [22] M. L. Miller, K. Reygers, S. J. Sanders, and P. Steinberg, “Glauber modeling in high energy nuclear collisions,” Ann. Rev. Nucl. Part. Sci. **57**, 205 (2007).
- [23] S. S. Adler *et al.* (PHENIX Collaboration), “Systematic studies of the centrality and $\sqrt{s_{NN}}$ dependence of the $dE_T/d\eta$ and $dN_{ch}/d\eta$ in heavy ion collisions at midrapidity,” Phys. Rev. C **71**, 034908 (2005), [Erratum: Phys. Rev. C **71**, 049901 (2005)].
- [24] R. Hofstadter, “Electron scattering and nuclear structure,” Rev. Mod. Phys. **28**, 214 (1956).
- [25] M. Luzum and P. Romatschke, “Conformal relativistic Viscous Hydrodynamics: Applications to RHIC Results at $\sqrt{s_{NN}}=200$ GeV,” Phys. Rev. C **78**, 034915 (2008), arXiv:0804.4015 [nucl-th].
- [26] K. Adcox *et al.* (PHENIX Collaboration), “PHENIX Central Arm Tracking Detectors,” Nucl. Inst. Methods Phys. Res., Sect. A **499**, 489 (2003).
- [27] J. D. Bjorken, “Highly Relativistic Nucleus-Nucleus Collisions: The Central Rapidity Region,” Phys. Rev. D **27**, 140 (1983).
- [28] S. Chatrchyan *et al.* (CMS Collaboration), “Measurement of the pseudorapidity and centrality dependence of the transverse energy density in PbPb collisions at $\sqrt{s_{NN}}=2.76$ TeV,” Phys. Rev. Lett. **109**, 152303 (2012).
- [29] C. Loizides (ALICE Collaboration), “Charged-particle multiplicity and transverse energy in Pb-Pb collisions at $\sqrt{s_{NN}}=2.76$ TeV with ALICE Collaboration,” Quark matter. Proceedings, 22nd International Conference on Ultra-Relativistic Nucleus-Nucleus Collisions, Quark Matter 2011, Annecy, France, May 23-28, 2011, J. Phys. G **38**, 124040 (2011).
- [30] K. Aamodt *et al.* (ALICE Collaboration), “Suppression of Charged Particle Production at Large Transverse Momentum in Central Pb-Pb Collisions at $\sqrt{s_{NN}}=2.76$ TeV,” Phys. Lett. B **696**, 30 (2011).
- [31] I. Vitev, “Testing the mechanism of QGP-induced energy loss,” Phys. Lett. B **639**, 38 (2006).

- [32] A. Adare *et al.* (PHENIX Collaboration), “Quantitative Constraints on the Opacity of Hot Partonic Matter from Semi-Inclusive Single High Transverse Momentum Pion Suppression in Au+Au collisions at $\sqrt{s_{NN}}=200$ GeV,” Phys. Rev. C **77**, 064907 (2008).